Hearing Research 364 (2018) 104–117

Contents lists available at ScienceDirect

Hearing Research

journal homepage: www.elsevier.com/locate/heares

Research Paper

Hidden hearing loss and endbulbs of Held: Evidence for central pathology before detection of ABR threshold increases

Michael A. Muniak [a, b, *, 1], Femi E. Ayeni [a, c, 1], David K. Ryugo [a, c, d]

[a] Hearing Research, Garvan Institute of Medical Research, Sydney, NSW 2010, Australia
[b] St Vincent's Clinical School, UNSW Sydney, Sydney, NSW 2052, Australia
[c] School of Medical Sciences, UNSW Sydney, Sydney, NSW 2052, Australia
[d] Department of Otolaryngology, Head, Neck & Skull Base Surgery, St Vincent's Hospital, Sydney, NSW 2010, Australia

ARTICLE INFO

Article history:
Received 27 November 2017
Received in revised form
22 February 2018
Accepted 18 March 2018
Available online 20 March 2018

Keywords:
Auditory brainstem response
Auditory nerve
Cochlear nucleus
Neurobiotin

ABSTRACT

Reductions in sound-evoked activity in the auditory nerve due to hearing loss have been shown to cause pathological changes in central auditory structures. Hearing loss due strictly to the aging process are less well documented. In this study of CBA/CaH mice, we provide evidence for age-related pathology in the endbulb of Held, a large axosomatic ending arising from myelinated auditory nerve fibers. Endbulbs are known to be involved in the processing of temporal cues used for sound localization and speech comprehension. Hearing thresholds as measured by auditory brainstem response (ABR) thresholds remained stable up to one year, whereas suprathreshold amplitudes of early ABR waves decreased by up to 50% in older mice, similar to that reported for age-related cochlear synaptopathy (Sergeyenko et al., 2013). The reduction of ABR response magnitude with age correlated closely in time with the gradual atrophy of endbulbs of Held, and is consistent with the hypothesis that endbulb integrity is dependent upon normal levels of spike activity in the auditory nerve. These results indicate that central auditory pathologies emerge as consequence of so-called "hidden" hearing loss and suggest that such brain changes require consideration when devising therapeutic interventions.

1. Introduction

The consequences of hearing loss are at times baffling. Classic hearing loss has elevated hearing thresholds and loss of sensory receptor cells (Schuknecht, 1974). In contrast, many affected listeners, especially the elderly, exhibit impaired temporal processing and difficulties understanding speech in noise without elevated thresholds or cognitive impairments (Dubno et al., 1984; Fullgrabe et al., 2014; Gordon-Salant, 2005; Gordon-Salant and Fitzgibbons, 1993; Ruggles et al., 2012; Snell and Frisina, 2000). Indeed, the physical substrate of age-related hearing loss in the absence of sensory receptor cell loss has remained "hidden" until quite recently (Liberman and Kujawa, 2017).

The CBA inbred mouse strain and its variants (e.g., CBA/J, CBA/Ca, CBA/CaJ, CBA/CaH) have long been used in hearing research (Berlin, 1963; Ohlemiller et al., 2016; Zheng et al., 1999). These mouse lines show minimal cochlear pathology and stable auditory brainstem response (ABR) thresholds over the first two years of life (Henry and Chole, 1980; Sergeyenko et al., 2013). Consequently, the CBA genotype has been widely accepted as representing normal hearing, and its auditory functions have routinely been compared with those of mice with various forms of hereditary hearing loss (e.g., Connelly et al., 2017; Limb and Ryugo, 2000; Willott, 1984, 1986; Willott et al., 1991). Recently, however, CBA/CaJ mice older than two years of age were observed to exhibit increased ABR thresholds, decreased ABR waveform amplitudes, and increased hair cell losses (Sergeyenko et al., 2013). Moreover, ribbon synapses between auditory nerve fibers and inner hair cells (IHCs) declined in number prior to spiral ganglion cell loss (Kujawa and Liberman, 2009; Stamataki et al., 2006). Thus, even in so-called "normal" hearing mice with a lifetime of non-damaging sound exposure, the cochlea may nonetheless exhibit "hidden" hearing loss as a result of age-related synaptopathy.

The causes of "hidden" and "overt" hearing loss generally originate in the cochlea. There is a growing consensus, however, that

Abbreviations: ABR, auditory brainstem response; AVCN, anteroventral cochlear nucleus; BC, bushy cell; CN, cochlear nucleus; EB, endbulb of Held; IHC, inner hair cell; SR, spontaneous rate

* Corresponding author. 384 Victoria St., Darlinghurst, NSW, 2010, Australia.
E-mail address: m@muniak.com (M.A. Muniak).

[1] Authors contributed equally to this work.

https://doi.org/10.1016/j.heares.2018.03.021
0378-5955/

many symptoms of hearing loss (e.g., difficulty understanding speech in noise, loudness distortion, and tinnitus) are exacerbated by reactive changes within the central nervous system (Parks et al., 2004). Changes in auditory nerve activity caused by hearing loss have a ripple effect throughout the central auditory pathway (Hashisaki and Rubel, 1989; Kral et al., 2005; Moore and Kowalchuk, 1988; Powell and Erulkar, 1962; Saada et al., 1996; Schwartz and Higa, 1982; Trune, 1982; West and Harrison, 1973), and pathologic changes are likely to first emerge at the cochlear nucleus (CN).

Auditory nerve endings terminate throughout the CN (Muniak et al., 2016), and have been a subject of extensive studies on deprivation-induced changes. In particular, attention has focused on endbulbs of Held (EBs; Held, 1893)—large, axosomatic endings of myelinated auditory nerve fibers that target bushy cells (BCs) in the anteroventral CN (AVCN). These synaptic endings are among the largest synapses in the brain (Ryugo and Spirou, 2009) and show evolutionary conservation across all vertebrates examined to date (Lenn and Reese, 1966; Ryugo and Parks, 2003). They are a crucial structure in the timing pathway, delivering auditory spikes at rapid rates and with high fidelity (Manis et al., 2011). Crucially, EBs have been shown to be structurally and functionally sensitive to changes in levels of spike activity, as would occur with deafness or hearing loss (Connelly et al., 2017; Ngodup et al., 2015; Oleskevich and Walmsley, 2002; Ryugo et al., 1996, 1997, 1998, 2005; Tsuji and Liberman, 1997; Wang and Manis, 2006; Zhuang et al., 2017). Thus, cochlear pathologies have the potential to cascade along ascending neural pathways, consequently producing deficits in central auditory processing (Frisina and Frisina, 1997; Lorenzi et al., 2006).

Age-related synaptopathy between auditory nerve fibers and IHCs (Sergeyenko et al., 2013) would render the affected primary fibers unresponsive to sound. Given the known role of activity on central synapse structure of the auditory nerve, we asked whether there would be a structural correlate of age-related hearing loss expressed centrally in EBs. We first examined our database of historical ABR records for CBA/CaH mice up to one year of age to corroborate and extend recent observations (Sergeyenko et al., 2013). Next, we examined EB morphology in a subset of these mice at specific age-groups. We hypothesized that age-related cochlear synaptopathy, as inferred from reductions in ABR waveform amplitudes, would result in atrophy of EB morphology reminiscent of observations in animals with overt hearing loss (e.g., Connelly et al., 2017; Limb and Ryugo, 2000; Ryugo et al., 1997).

2. Methods

2.1. Animals

All procedures were performed in accordance with NHMRC guidelines and approved by the Animal Ethics Committee of the Garvan Institute of Medical Research and St. Vincent's Hospital, UNSW Australia. A total of 22 normal hearing CBA/CaH mice of both sexes (11 male, 11 female) were used in this study. Age at time of study ranged from 4 to 52 wks. Ten mice were of the CBA/CaH genotype. The remaining 12 mice were transgenic CBGlyT2-EGFP mice, which expressed enhanced green flourescent protein (EGFP) under the influence of the glycine transporter 2 (GlyT2) gene promoter (Zeilhofer et al., 2005). Parent GlyT2–EGFP mice with a C57Bl/6 background were donated by Prof. H.U. Zeilhofer (University of Zurich, Switzerland). Congenic CBGlyT2-EGFP mice were obtained by backcrossing the transgene into CBA/CaH mice for at least 10 generations. All mice were bred in our colony at the Australian BioResources facility (Moss Vale, NSW, Australia). Pups were weaned from their mothers at 3 wks of age and transported to the animal care facility of the Garvan Institute of Medical Research. All mice were given standard chow (6% fat, 23% protein; Gordon's Specialty Stock Feeds, Yanderra, NSW, Australia) and water *ad libitum*.

Four of the CBA/CaH mice were monitored over their lifespan and continuously housed in standard cages in the animal care facility where the internal average ambient sound level was 60–65 dB SPL (RMS; 2–200 kHz filter). Mice were only exposed to normal everyday vivarium acoustics, and there were no overt damaging levels of sound. The remaining 18 mice were also reared and housed in standard conditions until they were selected for observation over an 8-wk period beginning at 4, 8, 12, 24, 32, or 44 wks of age. During this period, subjects were housed in acoustically treated sound boxes where the average ambient sound level was reduced to 47 dB SPL (RMS) and were instead exposed to a controlled sound environment delivered via an overhead speaker (MF1; Tucker Davis Technologies [TDT], Alachua, FL) mounted 26 cm above the floor of the mouse cage. Sounds consisted of randomized ultrasonic environmental recordings and synthesized frequency sweeps spanning the mouse hearing range (2–60 kHz). The average intensity of stimulus delivery, measured at the level of a mouse's head, was fixed to 55 dB SPL (RMS) and peak intensity was limited to 65 dB SPL. The sound stimulus was randomly interleaved with 50% silence and delivered daily between 7pm and 7am.

We also included ABR measurement data from an additional 147 CBA/CaH mice (55 male, 92 female) that were tested in our laboratory in relation to other experiments using identical procedures. Ages ranged from 3 to 44 wks of age. 127 of these mice were of the CBA/CaH genotype, and the remaining 20 were transgenic CBGlyT2-EGFP mice. Animals were either sourced from our colony at Australian BioResources or purchased from Animal Resources Centre (Canning Vale, WA, Australia). Normal vivarium housing conditions applied to all of these subjects. Due to the high variability of sampling at different age-groups, N-values are provided for each measurement in Tables 1 and 2.

2.2. Auditory brainstem responses

Mice were anaesthesised with 100 mg/kg ketamine and 20 mg/kg xylazine and placed on an infrared heating pad inside a sound-attenuating chamber (Sonora Technology, Gotenba, Japan). Ophthalmic ointment was applied to both eyes to prevent corneal irritation. ABRs were differentially recorded using subcutaneous platinum needle electrodes that were positioned over the vertex of the skull (active), the right bulla (reference), and muscle of the hind leg (ground). The right pinna was positioned 10 cm away from and at the same level as a free-field speaker (MF1). Alternating click (0.1 ms square wave pulse) and tone stimuli at 4, 8, 16, 24, 32, 40, and 48 kHz (5 ms duration, 0.5 ms rise/fall) were generated using a software-controlled signal processor (RZ6/*BioSigRZ*; TDT) and delivered at a rate of 10/s in 10-dB decremental steps from 90 dB to below any detectable response. Responses were amplified (RA16PA/RA4LI; TDT), bandpass filtered from 0.5 to 3 kHz, notched at 50 Hz, and averaged over 512 stimuli presentations (RZ6; TDT).

Following Sergeyenko et al. (2013), we will refer to individual components of the ABR as Waves 1–5 to distinguish them from Waves I–V as defined in larger mammals (Melcher and Kiang, 1996). Offline analysis of ABR readings began in *BioSigRZ*, where peak-to-trough positions of Waves 1–5 were manually marked. Data files were subsequently ported to a custom ABR viewer in *MATLAB* (vR2016a; MathWorks, Natick, MA) for further analysis. Response thresholds were independently determined by two observers using a blinded procedure: stacked waveform sets (e.g., Fig. 1A) were presented in random order with no identifying information (e.g., stimulus frequency, mouse id, mouse age), with the

Table 1
Summary of ABR thresholds.

		Threshold (dB SPL)															
		Click		*4 kHz*		*8 kHz*		*16 kHz*		*24 kHz*		*32 kHz*		*40 kHz*		*48 kHz*	
Age (weeks)	*4*	38.8 ± 5.2	(24)	73.1 ± 8.3	(13)	40.7 ± 11.0	(15)	25.7 ± 6.8	(15)	29.3 ± 11.6	(15)	38.3 ± 11.8	(15)	48.1 ± 8.3	(13)	53.3 ± 5.8	(3)
	8	38.9 ± 5.2	(19)	72.5 ± 7.6	(8)	36.7 ± 6.6	(9)	25.0 ± 5.0	(9)	27.8 ± 6.7	(9)	36.7 ± 4.3	(9)	49.4 ± 7.8	(8)	53.3 ± 5.8	(3)
	12	36.8 ± 4.6	(88)	65.9 ± 10.3	(32)	32.3 ± 8.0	(32)	23.0 ± 5.9	(32)	26.7 ± 7.6	(32)	36.8 ± 9.0	(30)	48.8 ± 10.0	(25)	67.1 ± 9.1	(7)
	16	39.2 ± 5.0	(24)	69.4 ± 9.8	(8)	36.2 ± 8.8	(8)	26.1 ± 8.2	(9)	30.0 ± 5.6	(9)	41.1 ± 10.5	(9)	49.4 ± 11.0	(9)	62.5 ± 9.6	(4)
	20	37.8 ± 6.7	(9)	72.5 ± 6.9	(6)	35.0 ± 6.3	(6)	25.0 ± 7.6	(8)	30.0 ± 9.6	(8)	40.6 ± 5.6	(8)	48.6 ± 10.3	(7)	65.0 ± 10.0	(4)
	24	40.0 ± 3.5	(17)	72.5 ± 10.0	(14)	40.7 ± 7.6	(14)	28.0 ± 6.2	(15)	33.9 ± 10.8	(14)	38.6 ± 8.1	(11)	44.5 ± 10.8	(11)	60.7 ± 8.4	(7)
	28	41.4 ± 4.1	(14)	72.3 ± 8.3	(13)	38.1 ± 8.8	(13)	29.6 ± 7.2	(13)	37.7 ± 9.3	(13)	44.1 ± 15.0	(11)	46.7 ± 9.7	(9)	64.2 ± 8.0	(6)
	32	43.0 ± 4.8	(10)	75.6 ± 8.8	(9)	37.8 ± 8.3	(9)	25.6 ± 5.3	(9)	32.5 ± 4.6	(8)	36.2 ± 4.4	(8)	43.3 ± 4.3	(9)	63.6 ± 4.8	(7)
	36	47.5 ± 4.2	(6)	75.8 ± 11.1	(6)	40.0 ± 6.3	(6)	30.0 ± 7.1	(5)	30.0 ± 0.0	(5)	40.0 ± 0.0	(6)	44.2 ± 9.2	(6)	62.0 ± 4.5	(5)
	40	42.5 ± 5.0	(4)	85.0 ± 5.8	(4)	45.0 ± 13.2	(3)	31.2 ± 2.5	(4)	36.7 ± 5.8	(3)	45.0 ± 10.0	(4)	50.0 ± 8.2	(4)	60.0 ± 0.0	(3)
	44	48.0 ± 4.5	(5)	78.0 ± 11.5	(5)	35.0 ± 5.0	(5)	31.2 ± 2.5	(4)	37.5 ± 9.6	(4)	48.3 ± 2.9	(3)	56.7 ± 5.8	(3)	66.7 ± 5.8	(3)
	48	45.0 ± 5.8	(4)	71.7 ± 7.6	(3)	37.5 ± 5.0	(4)	27.5 ± 5.0	(4)	37.5 ± 9.6	(4)	42.5 ± 5.0	(4)	46.7 ± 5.8	(3)	65.0 ± 15.0	(3)
	52	50.0 ± 0.0	(3)	70.0 ± 10.0	(3)	40.0 ± 0.0	(3)	30.0 ± 0.0	(3)	33.3 ± 5.8	(3)	36.7 ± 5.8	(3)	50.0 ± 10.0	(3)	66.7 ± 5.8	(3)

Values are mean ± SD. Sample size in parentheses.

Table 2
Summary of ABR amplitudes.

		Wave 1 Amplitude (μV)								Wave 2			
		Click		*8 kHz*		*16 kHz*		*24 kHz*		*Click*	*8 kHz*	*16 kHz*	*24 kHz*
Age (weeks)	*4*	5.21 ± 1.59	(24)	1.02 ± 0.48	(15)	2.11 ± 0.91	(15)	1.99 ± 1.06	(15)	6.92 ± 2.41	1.28 ± 0.61	2.14 ± 1.04	2.23 ± 1.18
	8	5.81 ± 1.53	(19)	1.01 ± 0.36	(8)	2.08 ± 0.52	(9)	1.95 ± 0.40	(7)	7.87 ± 2.09	1.62 ± 0.65	2.30 ± 1.18	2.07 ± 0.67
	12	6.28 ± 1.46	(88)	1.18 ± 0.36	(31)	2.19 ± 0.50	(29)	1.97 ± 0.49	(30)	8.06 ± 2.27	1.69 ± 0.59	2.02 ± 0.92	2.02 ± 0.65
	16	5.50 ± 1.39	(21)	1.18 ± 0.35	(8)	1.99 ± 0.32	(8)	1.77 ± 0.20	(8)	7.47 ± 2.10	1.75 ± 0.56	2.19 ± 0.52	1.88 ± 0.42
	20	5.22 ± 1.16	(8)	0.88 ± 0.17	(3)	1.82 ± 0.23	(6)	1.61 ± 0.31	(6)	6.98 ± 1.93	1.88 ± 0.43	2.01 ± 0.83	1.92 ± 0.65
	24	4.47 ± 1.25	(15)	0.97 ± 0.42	(11)	1.31 ± 0.50	(11)	1.47 ± 0.59	(11)	6.08 ± 1.56	1.33 ± 0.48	1.49 ± 0.63	1.59 ± 0.55
	28	3.35 ± 1.02	(13)	0.81 ± 0.27	(10)	1.25 ± 0.31	(10)	1.13 ± 0.40	(10)	4.89 ± 2.02	1.48 ± 0.65	1.48 ± 0.80	1.46 ± 0.67
	32	2.98 ± 1.30	(9)	0.46 ± 0.18	(9)	0.91 ± 0.30	(9)	1.03 ± 0.38	(9)	4.15 ± 1.75	0.96 ± 0.41	1.14 ± 0.67	1.30 ± 0.64
	36	2.17 ± 0.18	(4)	0.49 ± 0.14	(6)	0.85 ± 0.16	(6)	1.03 ± 0.10	(6)	2.65 ± 0.43	0.85 ± 0.20	0.81 ± 0.38	1.01 ± 0.16
	40	2.96 ± 1.50	(3)	0.48 ± 0.19	(4)	0.82 ± 0.28	(4)	0.83 ± 0.36	(4)	2.97 ± 1.56	0.60 ± 0.14	0.40 ± 0.20	0.87 ± 0.22
	44	2.43 ± 1.09	(4)	0.56 ± 0.26	(5)	0.78 ± 0.24	(5)	0.98 ± 0.38	(5)	3.24 ± 2.34	1.11 ± 0.34	0.93 ± 0.44	0.91 ± 0.45
	48	2.01 ± 0.24	(3)	0.41 ± 0.10	(4)	0.75 ± 0.11	(4)	0.85 ± 0.13	(4)	3.57 ± 0.49	0.86 ± 0.34	0.68 ± 0.09	0.63 ± 0.14
	52	1.87 ± 0.31	(3)	0.37 ± 0.18	(3)	0.74 ± 0.25	(3)	0.85 ± 0.17	(3)	3.46 ± 0.51	1.03 ± 0.12	1.05 ± 0.32	1.08 ± 0.29

Values are mean ± SD. Wave 1 sample sizes (in parentheses) also apply to Wave 2 measurements.

user required to manually select the lowest sound level that evoked a repeatable response waveform. Differences between the two observers were never greater than ±10 dB and were averaged. Waveform amplitude was calculated as the difference (in μV) between the peak and following trough of a given wave.

2.3. Cochlear surgery and auditory nerve injection

After the final ABR session, 17 mice were subjected to cochlear surgery and auditory nerve injection to label auditory nerve fibers and endings in the AVCN (Connelly et al., 2017). Mice were prepared for injection using aseptic techniques. Anesthesia was induced using isoflurane (5% in 0.6 L/min O_2) and maintained (1.5–2%) for the duration of the surgery. Each mouse was visually monitored for respiration rate, and checked for an eye and paw reflex prior to incision and throughout the procedure. Ophthalmic ointment was applied to both eyes to prevent corneal drying. The anesthetized mouse was secured in a nose cone with a bite bar and placed on its left side to ensure the right ear was facing upward. The hair behind the right ear was removed, skin swabbed with Betadine solution, and 0.01 mL bupivacaine applied around the exposed area. A posterior auricular incision was then made, the skin was raised, and subcutaneous tissue along the cartilaginous external auditory canal was reflected downward until the bulla was reached. Using a toothed forcep, the posterior inferior aspect of the bulla was chipped away to expose the otic capsule. At this junction, a blunt dissection was made into the cartilaginous external auditory canal so as to remove the tympanic membrane, malleus, and incus. The stapedial artery was then cauterized with a low-temperature cautery (Medtronic, North Ryde, NSW, Australia) at its inferior and superior portion so that the stapes could be freed from its attachment to the oval window membrane. After the stapes had been removed, a fine-end curved hook was inserted into the round or oval window to chip off the lateral wall of the otic capsule. The modiolus was located in the cochlea and an acupuncture needle was used to gently poke 2–3 holes in its apical and middle turns. A glass micropipette, 80–90 μm diameter, filled with 5% neurobiotin (SP-1120; Vector Laboratories, Burlingame, CA), was used to pressure-inject 5 μl of dye into the modiolus of cochlea (Nanoject II; Drummond Scientific Company, Broomall, PA). After allowing the dye to settle for 5 min, the pipette was subsequently withdrawn and incision suture closed. Animals were administered buprenorphine (0.05 mg/kg) and sterile saline (~0.5 mL) subcutaneously and allowed to survive for 4–6 h to permit tracer diffusion throughout the auditory nerve.

2.4. Tissue preparation

At the end of the survival time, animals were intraperitoneally administered a lethal dose of sodium pentobaribitone (55 mg/kg). When the animal was areflexic to a paw pinch, the thorax was opened to expose the heart and 0.02 mL heparinized saline was injected directly into the right ventricle to reduce clotting. The heart was then transcardically perfused through the left ventricle with 2 mL 1% $NaNO_2$ in 0.1 M phosphate buffered saline prewash, followed by 60 mL of 4% paraformaldehyde in 0.1 M phosphate

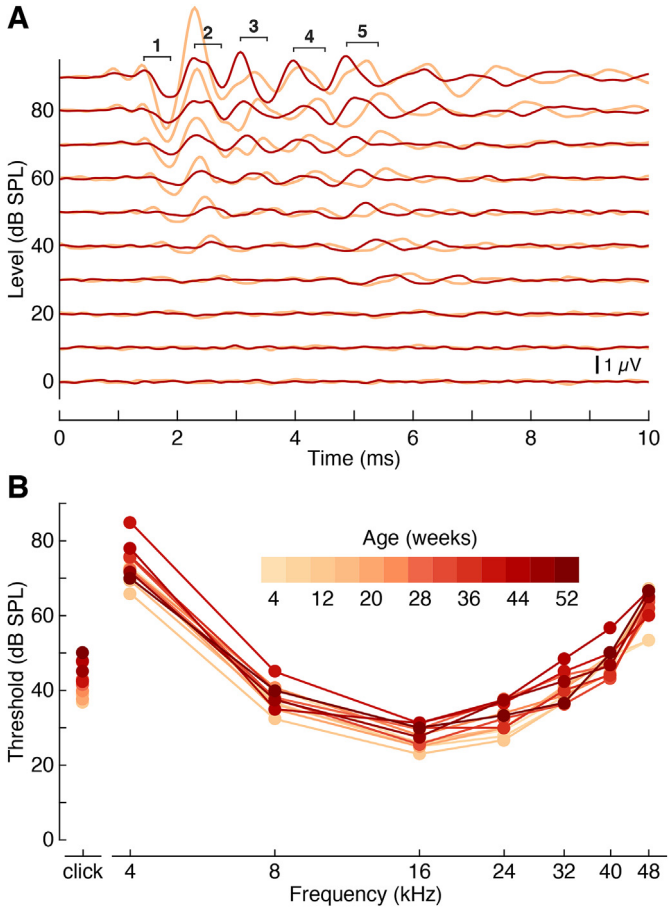

Fig. 1. CBA mice maintain normal hearing thresholds up to one year of age. (A) Example ABR waveforms (16 kHz; 0–90 dB SPL) from the same mouse at both 5 (tan) and 44 (red) wks of age. While threshold remains unchanged (30 dB SPL, late waves), a reduction in ABR amplitude is evident at 44 wks versus 5 wks, particularly for Waves 1 and 2. Black bars indicate the peak-to-trough intervals of Waves 1–5 at 44 wks and 90 dB SPL. **(B)** Mean ABR freefield audiograms for CBA mice at 4-wk intervals from 4 to 52 wks of age. Click and tone thresholds exhibit only a modest elevation with age. Values are summarized in Table 1.

buffered saline solution (pH 7.4). The head was post-fixed overnight at room temperature in the same fixative on a shaking platform. The following day, the brain was dissected from the skull, and the brain stem was isolated and embedded in a gelatin-albumin mixture. Coronal sections were cut at 50 μm with a vibrating microtome (VT1200S; Leica Systems, Nussloch, FRG) and free-floating tissue sections were collected in 0.12 M Tris buffer (TBS). Thereafter, tissue sections were incubated with streptavidin conjugated to Alexa Fluor 568 (1:1000; S-11226; Life Technologies, Scoresby, VIC, Australia) in 0.12 M TBS for 1 h to visualize neurobiotin-filled EBs in the AVCN. After incubation, tissue sections were rinsed thrice in 0.12 M TBS for 5 min, mounted on microscope slides, and coverslipped using Vectashield (H-1400; Vector Labs, Burlingame, CA). Slides from all mouse cohorts were intermixed and coded by a neutral party so that the observer was blinded to the ages of the subjects throughout analyses.

2.5. Confocal image acquisition and analysis

Z-stack images of coded tissue sections were acquired with a confocal microscope (DMI 6000 SP8; Leica Systems; objective: 63×/1.20 water immersion, NA: 1.2, pinhole: 1 Airy unit), using laser excitation at 561 nm (intensity: 15%), at a resolution of 1024 × 1024 pixels, a z-step size of 0.35 μm, and a setting of one frame and line averaging. Only EBs with an identifiable axon and complete endings were imaged. The EB is identified as a large complex ending of the auditory nerve in the AVCN that surrounds the silhouette of a bushy cell body. The confocal parameters for image acquisition were kept constant for all cases.

After image acquisition, endbulb z-stacks were ported to *Imaris* software (v7.2; Bitplane, Zurich, Switzerland). This software allowed the visualization of the EB in 3-dimensional space based on fluorescence intensity and size (Fogarty et al., 2013). No image processing was done other than median filtering. We first reduced background noise using a median filter (3 × 3 × 3); the same filter was applied to all images and image edges were not altered (Ronneberger et al., 2008). Next, a solid surface of an EB was created in "surpass view" followed by the delineation of the segment of interest in the image plane. We disabled the "smoothing" tool in the software as this caused artificial uniformity of a surface, but enabled the background subtraction option (Fogarty et al., 2013). The software automatically determined the minimum branch diameter of the EB structure. This step was followed by manual thresholding of the EB fluorescence signal; a threshold value was chosen that was low enough to completely detect the EB of interest and its fine details. Following thresholding, a solid rendition of EB structure was created for quantification. The surface area and volume of each EB was calculated in *Imaris* after excluding the axon segment.

2.6. Statistical analyses

Statistical tests were conducted using *R* (v3.4.3; R Core Team., 2017). Physiology data (e.g., threshold, amplitude) were evaluated using multiple linear regression. Unless otherwise stated, additive models were employed with age as a continuous predictor along with categorical predictors of stimulus type (e.g., click, 8 kHz), genotype (CBA/CaH vs. CBGlyT2-EGFP), and housing condition (vivarium vs. sound box); baseline reference categories for coefficient reporting were "click", "CBA/CaH", and "vivarium". The relative importance of regressors was calculated with the *R* package *relaimpo* (v2.2-2; Grömping, 2006) following the "lmg" method (Lindeman et al., 1980, p.119ff), which averages the sequential sum of squares over orderings of regressors. Cross-sectional conditional plots with partial residuals were visualized with assistance of the *R* package *visreg* (v2.4-1; Breheny and Burchett, 2017). Endbulb data were not normally distributed, and group mean comparisons were made using the Kruskal-Wallis one-way ANOVA followed by Dunn's post-hoc test for multiple comparisons with the Holm-Šidák correction via the *R* package *dunn.test* (v1.3.5; Dinno, 2017). The distribution of endbulb data was examined for unimodality using Hartigans' dip test statistic with the *R* package *diptest* (v0.75-7; Maechler, 2016). Probability density functions for endbulb data were computed in *MATLAB* with an adaptive kernel density estimator (Botev et al., 2010). All error values correspond to the standard deviation (SD) unless otherwise indicated. Statistical significance was accepted at $p < 0.05$. Any use of the term "monthly" specifically denotes 4-wk intervals.

3. Results

3.1. Auditory brainstem response

ABRs were collected from mice beginning at various age points until they were terminated. Most mice used specifically for this study underwent ABR testing at multiple ages (range: 1–45 wks duration between first and last reading; median 9 wks duration). Results were assessed in 4-wk intervals; if a mouse was tested more

than once within a specific age group (e.g., 7–10 wks of age) only one sample from that timeframe was included for analysis. Of the 147 additional subjects that were included from historical laboratory records, only 5 contributed readings for more than one age group (2–4 readings each).

Four animals were followed on a near-weekly basis over their lifetime from 5 wks up to at least 32 wks of age—one mouse was observed until 49 wks—which allowed for direct age comparisons of ABRs in the same animal. Fig. 1A shows responses to 16-kHz tone pips at both 5 (tan) and 44 (red) wks of age in a single subject; thresholds were typically unchanged over this time frame (note the repeatable late response at 30 dB SPL), but waveform amplitudes were considerably diminished.

Audiograms were created for each age group (Fig. 1B) based on mean ABR thresholds from our dataset (Table 1). A remarkable consistency was observed over time and stimulus frequency—mean thresholds never deviated more than ±15 dB from 4-wk-old readings (mean: 9.7 ± 2.6 dB), and varied at most by 20 dB between lowest and highest readings for a given frequency (mean range: 12.9 ± 3.0 dB). To test whether age and/or stimulus type were accurate predictors of ABR threshold, we performed multiple linear regression. Furthermore, we included two additional predictor terms describing genotype and housing conditions in order to account for the heterogeneous distribution of our subjects with respect to these parameters (see Sections 2.1 and 2.6); we predicted these additional parameters would have no bearing on measurement outcomes. The resultant linear model adequately predicted threshold values (adj. $R^2 = 0.75$, $F(10,1013) = 309.8$, $p < 0.001$) largely on the basis of stimulus type (Fig. S1A; $\beta_{4kHz} = 31.8$, $p < 0.001$; $\beta_{8kHz} = -2.7$, $p = 0.002$; $\beta_{16kHz} = -13.4$, $p < 0.001$; $\beta_{24kHz} = -8.6$, $p < 0.001$; $\beta_{40kHz} = 8.0$, $p < 0.001$; $\beta_{48kHz} = 22.3$, $p < 0.001$) which accounted for 97% of the explained variance. However, age was also a significant predictor ($\beta_{age} = 0.15$, $p < 0.001$), supporting our observation that ABR thresholds tended to increase across the mouse's range of hearing by ~7–8 dB over the first year. Neither genotype nor housing condition were significant predictors (Figs. S1B–C), validating the inclusion of all mice in our dataset.

We limited subsequent analyses to responses for clicks and 8-, 16-, and 24-kHz tone pips, as suprathreshold waveforms were most robust for these stimuli. Mean ABR thresholds were first replotted longitudinally (Fig. 2A), which highlights their slight increase over the course of a year relative to 4-wk readings (Fig. 2B). A model fit to this threshold shift data (adj. $R^2 = 0.14$, $F(6,604) = 17.58$, $p < 0.001$) reaffirmed that age was a significant predictor for the modest elevation in threshold over one year (Fig. 2B; $\beta_{age} = 0.17$, $p < 0.001$). Additionaly, despite normalization, responses to 8-kHz tones remained slightly offset to those of other stimuli (Fig. S1D; $\beta_{8kHz} = -4.8$, $p < 0.001$), which is likely due to the slightly elevated mean response to 8 kHz at 4 wks relative to successive age groups. The primary regressor groups of age and stimulus type were deemed to have roughly equal importance to this model (45–46% each). As before, neither genotype nor housing condition factored into response variability (Figs. S1E–F).

Compared to the relatively mild threshold elevations detected in our aging animals, far more dramatic changes were observed for suprathreshold ABR waveform amplitudes. Fig. 3 shows the first 3 ms of the mean ABR waveform for each age group to 80-dB SPL stimuli, demonstrating a decline in mean amplitudes for Wave 1 and 2 across the first year of life (Table 2). Absolute amplitude values were extremely different for each stimulus—click-response waveform amplitudes were routinely 2-3x greater than tonal responses (Fig. 2C,E)—necessitating normalization of these values relative to 4-wk-old measurements to facilitate meaningful comparisons. The adjusted results (Fig. 2D,F) suggest that nearly all ABR waveforms declined at similar rates with age. By 52 wks of age, mean Wave 1 amplitudes for each stimulus were <50% of 4-wk values, with most responses crossing this threshold by 36 wks (Fig. 2D). This decrease was also reflected in Wave 2 amplitudes, albiet with more variability (Fig. 2F). A direct comparison of normalized Wave 1 vs. Wave 2 amplitudes at each age (Fig. 4A) further demonstrated that both waves show nearly identical declines in amplitude with age, except for 8-kHz Wave 2, which appeared to lag behind Wave 1 but reduced at a similar rate.

Linear models were again employed to test the hypothesis that age was a significant predictor for the decline of normalized ABR wave amplitudes. Indeed, the model for Wave 1 (adj. $R^2 = 0.46$, $F(6,561) = 82.82$, $p < 0.001$) suggested that age accounted for approximately 58% of the explained variance ($\beta_{age} = -0.015$, $p < 0.001$). Additionally, predicted responses were somewhat stratified by stimulus type, with responses to 16- and 24-kHz stimuli offset from click and 8-kHz responses (Fig. S2A; $\beta_{16kHz} = -0.14$, $p < 0.001$; $\beta_{24kHz} = -0.13$, $p < 0.001$), which is likely attributable to the divergence of mean response values at 12–24 wks (Fig. 2D). While genotype remained an unimportant factor (Fig. S2B), the model suggested that mice housed in our controlled sound environment would tend to have lower amplitudes relative to those allotted to the normal vivarium (Fig. S2C; $\beta_{housing} = -0.22$, $p < 0.001$), with this factor accounting for 20% of the explained variance. We were perplexed by this result, as housing conditions were designed to be relatively similar with respect to overall sound intensity, and this factor did not appear to impact hearing thresholds (Figs. S1C and F), ruling out overt cochlear damage. To explore this relationship further, we computed an alternate model with an additional interaction term (age:-housing). The output of this model (adj. $R^2 = 0.47$, $F(6,560) = 71.96$, $p < 0.001$) found a somewhat significant interaction ($\beta_{age} = -0.017$, $p < 0.001$; $\beta_{housing} = -0.32$, $p < 0.001$, $\beta_{age:housing} = 0.004$, $p < 0.05$) and suggested that, if anything, vivarium-housed animals tended to start with larger amplitudes at young ages compared to those in sound boxes (Fig. S2C'), but that values from both groups would nonetheless converge by 52 wks. Importantly, amplitude predictions declined by >50% for both levels of this factor—mirroring group mean observations—indicating that even if housing conditions truly affected waveform amplitudes, the observed decline with age remained the dominant effect.

The model for Wave 2 exhibited similar tendencies as that for Wave 1 (adj. $R^2 = 0.39$, $F(6,561) = 52.25$, $p < 0.001$), with age accounting for 35% of the explained variance ($\beta_{age} = -0.011$, $p < 0.001$). Predictions were somewhat stratified by stimulus type (Fig. S2D; $\beta_{8kHz} = 0.17$, $p < 0.001$; $\beta_{16kHz} = -0.13$, $p < 0.001$; $\beta_{8kHz} = -0.15$, $p < 0.001$), but not by genotype (Fig. S2E). Housing condition appeared to be a significant predictor (Fig. S2F; $\beta_{housing} = -0.23$, $p < 0.001$), but as with the model for Wave 1, we believe this can be attributed to the differential distribution of samples with respect to age (Fig. S2F').

To examine whether early (Waves 1–2) ABR waveform amplitude declines were reflected in later, more central components of the response, we also calculated mean Wave 5:1 and Wave 5:2 ratios for each age group, and plotted them relative to mean ratios at 4 wks of age (Fig. 4B–C). While there was considerable variability, owing in part to the difficulty in accurately measuring Wave 5, a clear trend of increasing ratio values was apparent, and not a single ratio declined with age. A linear model fit to Wave 5:1 data (on a $\log_2$ scale) reflected this variability (adj. $R^2 = 0.13$, $F(6,561) = 15.03$, $p < 0.001$), where the only major predictor was age ($\beta_{age} = 0.022$, $p < 0.001$) and suggested this ratio doubled from 4 to 52 wks. Wave ratios to 8-kHz tones exhibited a slight offset ($\beta_{8kHz} = 0.21$, $p = 0.02$), but all other predictors were deemed unimportant (Figs. S3A–C). A model fit to Wave 5:2 data (adj.

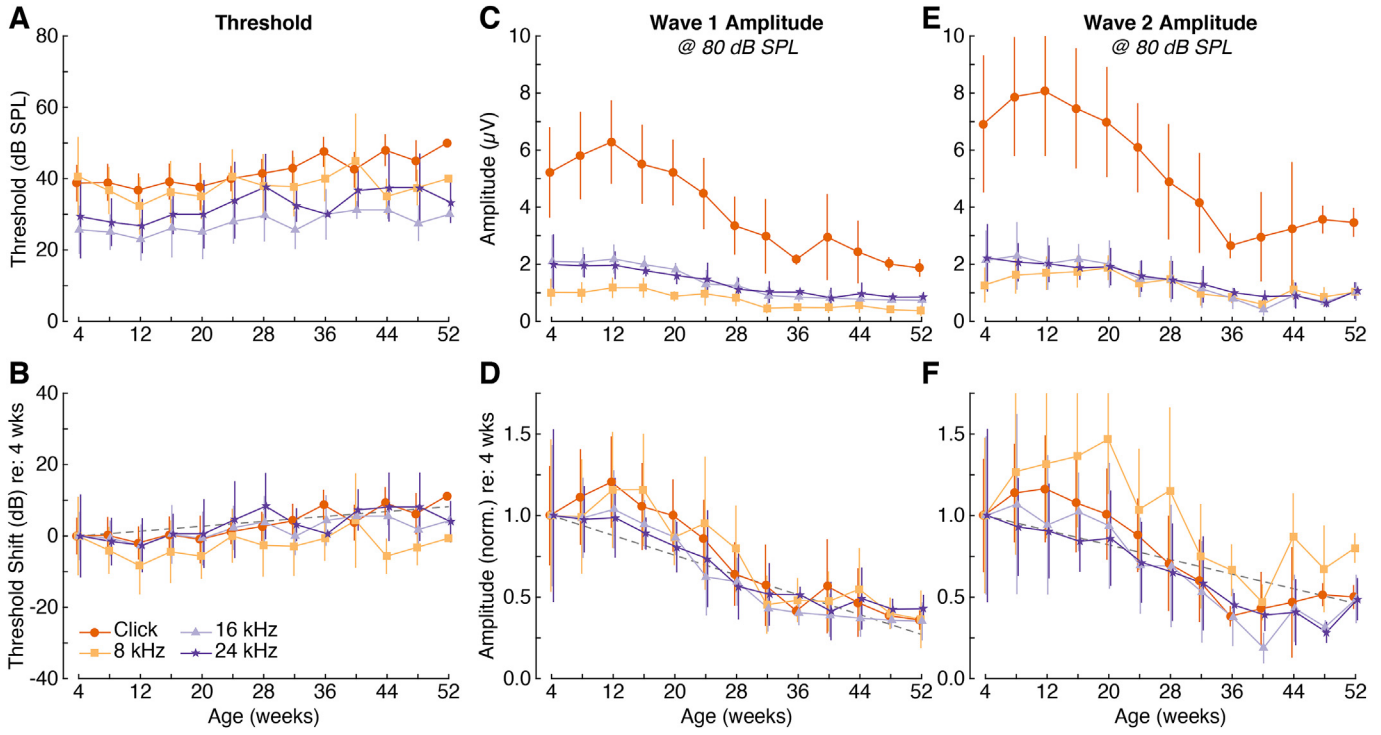

Fig. 2. Age-related changes in ABR waveforms across frequencies. Mean ABR measurements at 4-wk intervals from 4 to 52 wks of age are shown for click and 8-, 16-, and 24-kHz stimuli presented at 80 dB SPL. Top row (**A, C, E**) shows absolute means ± SD, bottom row (**B, D, F**) replots these data following normalization by subtracting (B) or dividing by (D, F) mean 4-wk-old values. Hearing thresholds (A–B) exhibit relatively minor shifts within the first year of age, and vary within a ±10 dB window. In contrast, wave 1 amplitudes (C–D) begin to decline after 12 wks of age, and drop to approximately half of their original value after 36 wks. Wave 2 amplitudes (E–F) also decline with age, following a similar trend to Wave 1. Dashed lines (B, D, F) show the partial effect of age from multiple regression, with the 4-wk value fixed to 0 dB (B) or 1.0 (D, F). Values are summarized in Table 2.

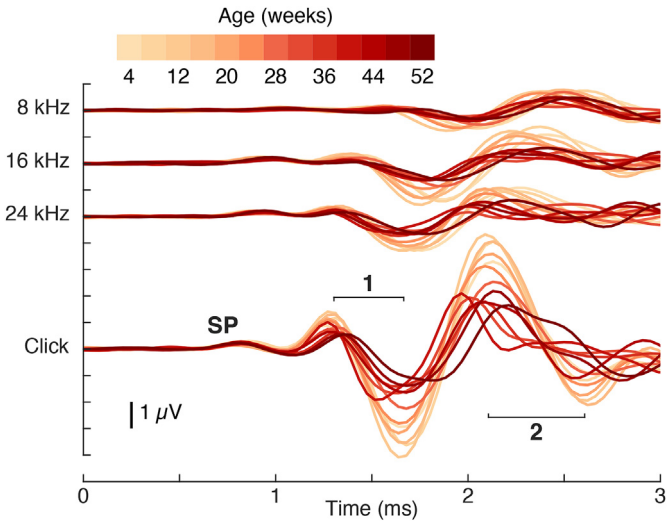

Fig. 3. ABR waveforms in aging mice show a reduction in amplitude. Mean ABR waveforms at different ages are shown for click and 8-, 16-, and 24-kHz stimuli presented at 80 dB SPL. The first 3 ms contains both cochlear (summating potential [SP], Wave 1) and early brainstem (Wave 2) components of the ABR. Horizontal lines indicate mean peak-to-trough duration for Waves 1 and 2 at 12 wks of age where mean amplitudes were largest. A gradual reduction in amplitude with age is evident for both Waves 1 and 2.

$R^2 = 0.013$, $F(6,561) = 10.03$, $p < 0.001$) also found age to be a significant factor in predicting ratio values ($\beta_{age} = 0.05$, $p < 0.001$; Figs. S3D–F) and suggested a ~50% increase from 4 to 52 wks.

3.2. Endbulbs of Held

Cochlear injections of neurobiotin were made in 17 animals at 12, 16, 20, 40, or 52 wks of age (Fig. 5A). Of these animals, 12 mice had also contributed longitudinal ABR data, whereas the remaining 5 were age-matched mice. All of these subjects were housed in the controlled acoustic environment for 8 wks prior to injection. After histological processing, labeled auditory nerve fibers and their endings were successfully recovered in 13 subjects. Labeled EBs were identified based on published criteria (Limb and Ryugo, 2000; Lorente de Nó, 1981; Ryugo and Fekete, 1982), and were the largest endings in the AVCN. Each EB was composed of a primary axon stalk that branched and gave rise to a complex axosomatic arbor that exhibited multiple *en passant* and terminal swellings (Fig. 5B). Well-isolated EBs were selected for 3D reconstruction and analysis using *Imaris* (Fig. 5C). Importantly, all analyses were performed on blinded slides; the observer had no knowledge as to the identity or age of any subject until all analyses were completed. At least 50 EBs were collected from each age group (Table 3), with a total of 349 EBs included in our analyses.

EBs exhibit a wide variety of shapes and sizes (Fig. 6). For each reconstructed EB we calculated its surface area and volume. EB surface area measurements ranged from 35.6 to 622.0 μm^2 (mean: 141.7 ± 74.2 μm^2; median: 128.0 μm^2). When grouped by age, a slight reduction in surface area was evident in older animals (Table 3; Fig. 7A). Notably, extremely large surface areas were only seen in younger animals. Probability density functions fit to the these values (Fig. 7A) were suggestive of a multimodal distribution, but statistical tests (see Section 2.6) failed to reject the null hypothesis (unimodal) in all instances. A one-way ANOVA showed significant variability ($p = 0.03$), with post-hoc comparisons indicating that mean EB surface area for 12- and 16-wk-old subjects

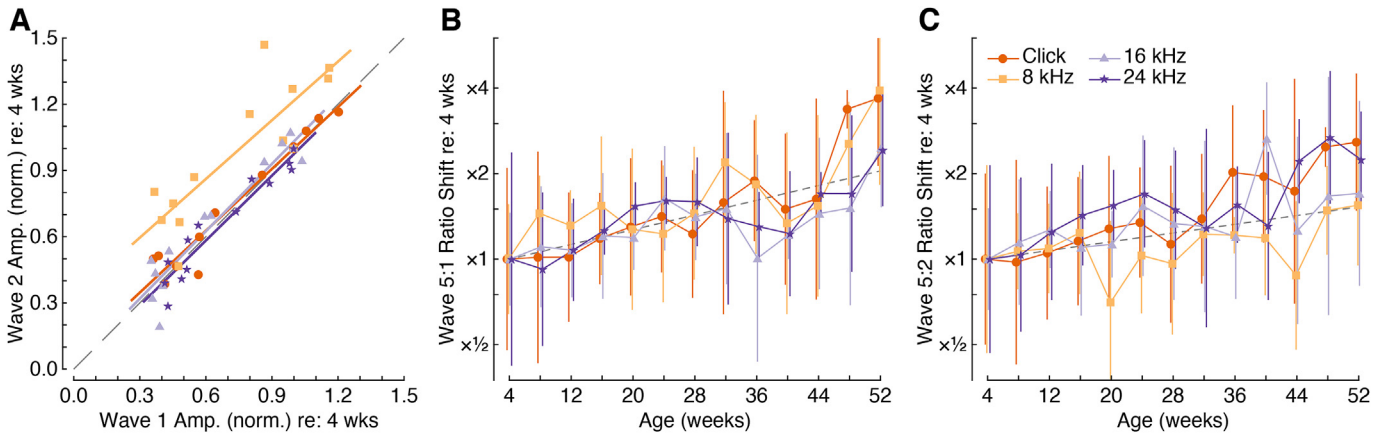

Fig. 4. Early ABR waves decrease more rapidly than later waves in older animals. Results are shown for responses to click and 8-, 16-, and 24-kHz stimuli presented at 80 dB SPL. **(A)** Comparison of mean normalized Wave 1 and 2 amplitudes from all age groups. Nearly all results fall on the identity line (dashed), indicating age-related reductions of Wave 2 occur in concert with Wave 1. The vertical offset of 8-kHz results would suggest similar rates of decline for both waves coupled with consistently stronger Wave 2 responses. **(B–C)** Mean ± SD shift in Wave 5:1 (B) and Wave 5:2 (C) ratios at 4-wk intervals from 4 to 52 wks of age relative to the mean 4-wk value. Data are plotted on a logarithmic axis; a 200% increase is equivalent in distance to a 50% decrease. Dashed lines show the partial effect of age from multiple regression, with the 4-wk value fixed to 1×. All ratios increase with age.

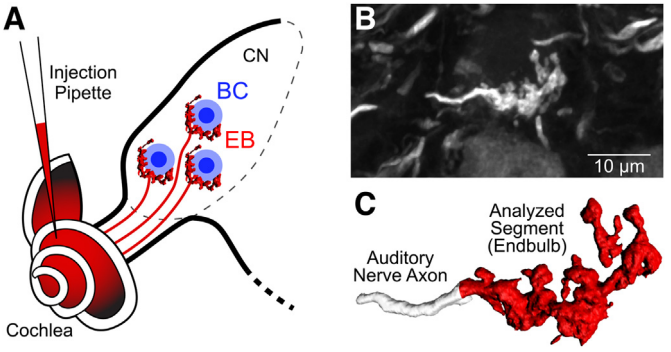

Fig. 5. 3D reconstruction of the endbulb of Held. (A) Schematic of injection protocol. Neurobiotin (red) is injected in the cochlea (see Section 2.3) where it is taken up by auditory nerve fibers. In the anteroventral cochlear nucleus (CN), auditory nerve fibers give rise to endbulbs of Held (EB) that terminate on bushy cells (BC). **(B)** Confocal photomicrograph (maximum z-projection) of a labeled EB. **(C)** 3D reconstruction of ending from (B), showing the incoming axon (white), and analyzed segment (EB; red). (For interpretation of the references to colour in this figure legend, the reader is referred to the Web version of this article.)

was significantly larger than 52-wk-old subjects ($p = 0.03$).

EB volume measurements ranged from 9.9 to 145.0 μm^3 (mean: 41.1 ± 21.1 μm^3; median: 36.2 μm^3). In contrast to surface area, a one-way ANOVA showed no significant variation ($p = 0.33$) in mean EB volume when grouped by age (Table 3; Fig. 7B). Indeed, large EB volumes were observed at both young and old age groups. As with surface area, we were unable to reject the hypothesis that measurements for each age group arose from unimodal distributions.

In order to evaluate the complexity of EB morphology with respect to age, we calculated a "shape factor" for each endbulb. The shape factor is a dimensionless quantity that describes the shape of a particle independent of its size and is calculated as $(SA^{1.5})/(6\sqrt{\pi}V)$, where SA and V are the EB surface area and volume, respectively (DeHoff, 1978). A shape factor of 1.0 represents a perfect sphere, whereas larger values typify more complex structures. EB shape factor measurements in our dataset ranged from 1.65 to 10.06 (mean: 3.85 ± 1.27; median: 3.65). When grouped by age, there was a notable decrease in mean EB shape factor with age (Table 3; Fig. 7C). A one-way ANOVA showed significant variation ($p < 0.001$), and post-hoc comparisons indicated that 12-wk ($p < 0.001$), 16-wk ($p = 0.003$), and 40-wk ($p = 0.02$) EBs were all significantly more complex in shape compared to that of 52-wk EBs. Once again, we could not reject the hypothesis that these values arose from unimodal distributions. A direct comparison of individual volume and shape factor measurements for all EBs (Fig. 8) suggests that a mean reduction in surface area is the causative factor in producing less complex EBs in older animals.

4. Discussion

In this study, we investigated the effects of age-related hearing loss on the morphology of EBs in the AVCN of mice. It was hypothesized that "hidden" hearing loss—a net reduction in sound-evoked activity in the auditory nerve in the absence of threshold shifts (Liberman and Kujawa, 2017)—would result in measurable changes in EB structure, producing a moderate version of EB pathology observed in mice with progressive acquired hearing loss (Connelly et al., 2017) or congenital deafness (Limb and Ryugo,

Table 3
Summary of endbulb of Held measurements.

		Sample Size	Surface Area (μm^2)	Volume (μm^3)	Shape Factor
Age (weeks)	*12*	54	168.1 ± 113.8*	45.1 ± 26.8	4.40 ± 1.78‡
	16	104	146.9 ± 69.7*	42.3 ± 20.5	3.92 ± 1.17†
	20	62	138.0 ± 59.9	39.4 ± 16.6	3.84 ± 1.14
	40	54	135.4 ± 52.7	39.1 ± 17.3	3.85 ± 0.94*
	52	75	123.1 ± 63.1	39.3 ± 23.2	3.35 ± 1.10

Values are mean ± SD.
Significance compared to 52-wks: * = $p < 0.05$, † = $p < 0.01$, ‡ = $p < 0.001$.

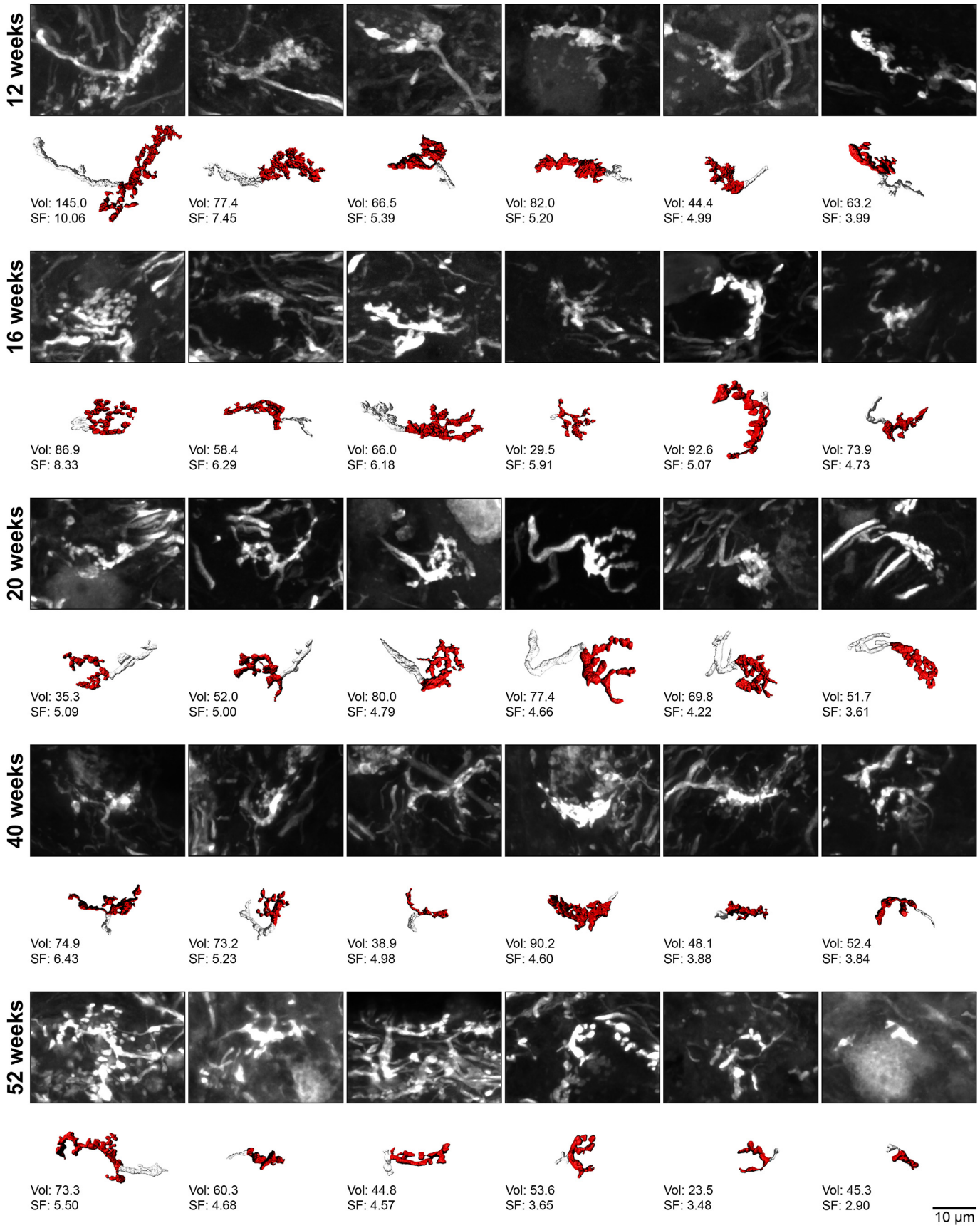

Fig. 6. Examples of reconstructed endbulbs of Held from 12 to 52 wks of age. For each age group, top row shows six representative confocal photomicrographs (maximum z-projection), and bottom row shows the corresponding 3D reconstruction. The analyzed endbulb segment is highlighted in red, with volume (μm^3) and shape factor values given for each example. Scale bar applies to all images. (For interpretation of the references to colour in this figure legend, the reader is referred to the Web version of this article.)

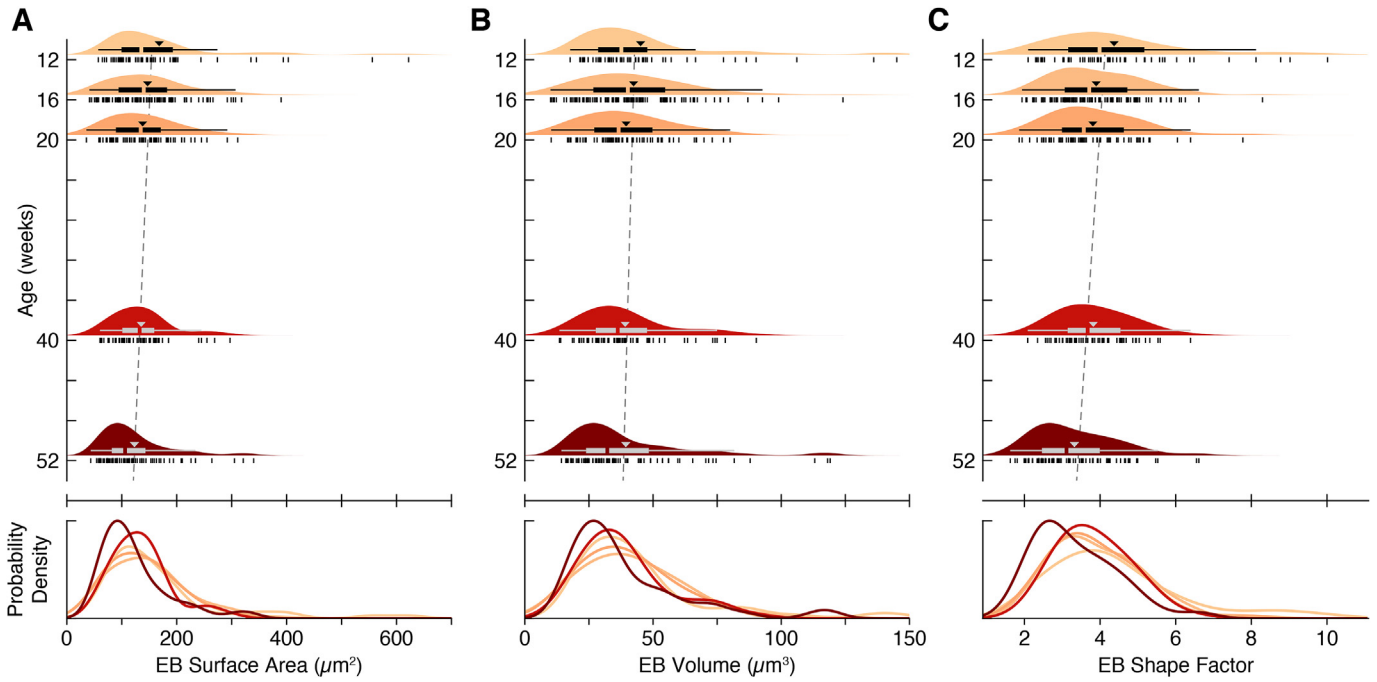

Fig. 7. Endbulbs of Held exhibit a less complex shape with age. Measurement profiles are shown for endbulb surface area (**A**), volume (**B**), and shape factor (**C**). The distribution of raw measurements for each age group are presented as a rug plot (black ticks), along with an estimated probability density function and a box-and-whisker plot with 1.5 interquartile range. Mean is indicated by a triangle. Dashed-line shows linear regression. Probability density functions are overlaid and expanded vertically at bottom. Values are summarized in Table 3.

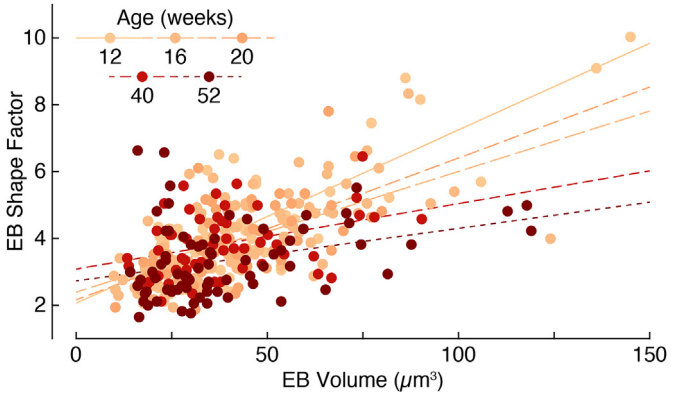

Fig. 8. Comparison of volume and shape factor values for each endbulb. Lines indicate linear regression for each age group. Endbulb shape factor tends to decrease with age relative to endbulb volume, suggesting endbulbs become less complex due to a reduction in surface area.

2000). We first examined the mean historical ABR profile of all CBA/CaH mice in our laboratory and show that response thresholds show only minor elevations up to one year of age. Despite this superficial preservation of hearing, suprathreshold amplitudes of early ABR waveforms dropped by 50% over this timeframe across a range of tested stimuli, suggesting a generalized impairment in signal transmission from the periphery to the central auditory system. We then reconstructed and analyzed labeled EBs in a subset of these mice and show that, on average, EBs show signs of reduced structural complexity in one-year-old mice. These results further support the idea that EBs are sensitive to changes in auditory nerve activity, including reductions that accompany “hidden” hearing loss.

4.1. Sample complexity

To establish a broad portrait of age-related hearing loss in CBA/CaH mice, we included animal data from a variety of sources in our laboratory beyond those explicitly earmarked for this study (see Section 2.1). This inclusiveness came at the cost of complexity with respect to sample numbers, genotype, and housing conditions. Unbalanced sample numbers reflect the typical usage of animals in our laboratory; most studies were not focused on aging, and accordingly utilized animals from 1 to 4 months of age for convenience. As a result, our sample numbers for physiological measurements were heavily skewed towards younger animals. Nonetheless, we observed clear changes in ABR waveform amplitude with respect to age that corroborated published results (Sergeyenko et al., 2013).

Our laboratory developed transgenic CBGlyT2-EGFP mice to facilitate anatomical studies of inhibitory projections in normal hearing mice. While parent GlyT2-EGFP mice originated from a C57Bl/6 background (Zeilhofer et al., 2005)—a strain noted for late-onset auditory degeneration (Henry and Lepkowski, 1978)—we backcrossed this transgene into our CBA/CaH mice for >10 generations to produce a congenic strain. We have since used both CBA variants interchangeably in our laboratory. Nonetheless, the insertion site of the transgene is as yet unmapped, and it is theoretically possible, though highly unlikely, that some genetic element associated with premature hearing loss in the C57 strain, such as *Ahl* (Johnson et al., 1997), could flank the transgene and thus carry over into our congenic line. There is no evidence, however, that aged hearing is abnormal in our CBGlyT2-EGFP animals. C57Bl/6 mice exhibit marked threshold increases above 16 kHz at one year of age (Parham, 1997). In contrast, the majority of our subjects at 52 wks belonged to the congenic line, and we only observed modest increases in thresholds across the board (Figs. 1–2). Furthermore, we included a categorical factor that accounted for genotype in all of

our regression analyses, and never found evidence for discrepancies between these populations (Figs. S1–S3). As such, we consider our CBGlyT2-EGFP animals to be equivalent to CBA/CaH with respect to hearing ability.

The last element of complexity in our study arose from differing housing conditions used for a subset of our mice. We designed acoustic sound boxes that allow for specific 24/7 control of the acoustic environment (e.g., deprivation, selective amplification). The subset of mice used in this study, however, were only subject to a "normal" sound environment that was designed to be similar to the vivarium of the animal care facility in terms of sound intensity and spectral content. We did not expect these mice to vary in their hearing ability compared to those housed in the normal vivarium, and indeed no differences were detected with respect to thresholds (Fig. S1). The discrepancy in ABR wave amplitudes between these two groups highlighted by regression analysis was surprising (Fig. S2), but subsequent investigation leads us to believe that this effect can be explained by the highly unbalanced sampling of mice in our study with respect to housing condition at young and old ages. At ages <36 wks, 84% of measurements arose from mice housed in the vivarium, compared to only 28% at ages $\geq$ 36 wks. Considering that these age ranges also correspond with larger vs. smaller amplitude values, respectively, it is no surprise that our model would report a bias for this predictor. Accordingly, we are confident that housing condition was not a materially relevant factor in the decline of early ABR wave amplitudes with age in our dataset, and that this reduction occurred in both groups.

4.2. Audiometric measurements

CBA inbred mice have been widely used as models of normal hearing (Berlin, 1963; Ohlemiller et al., 2016; Zheng et al., 1999) owing to their stable ABR thresholds up to two years of age (Henry and Chole, 1980; Li and Borg, 1991; Sergeyenko et al., 2013). Yet threshold elevations are still eventually observed, even in mice that have never experienced damaging sound exposures (Sergeyenko et al., 2013), suggesting age-related pathologies are an inevitable component of "normal" hearing. We observed, at most, a minor (+10-dB) shift in thresholds of one-year-old mice compared to 4-wk-old subjects. As our ABR protocol only varied stimuli in 10-dB increments, we may have overlooked more subtle shifts. Nonetheless, our results are consistent with previous reports (Henry and Chole, 1980; Li and Borg, 1991; Sergeyenko et al., 2013). It is also reasonable to assume that inner and outer hair cells are largely intact in our mice based on their age (Sergeyenko et al., 2013; Spongr et al., 1997).

Prior study identified marked reductions to suprathreshold ABR Wave 1 amplitudes in extremely old mice, but also showed that this descending trend started earlier in life (Sergeyenko et al., 2013). Indeed, our monthly snapshots of ABR measurements clearly indicate that a significant downturn in Wave 1 amplitude begins approximately midway through the first year. The first component of the ABR waveform corresponds to the summed activity of auditory nerve fibers (Melcher and Kiang, 1996). Ergo, a reduction in Wave 1 in our study could indicate dysfunction in sound encoding at any stage up to and including spiral ganglion cell activation. Because thresholds are unchanged, and given the assumption that outer hair cell are functioning normally—a similar cohort of mice showed no changes in distortion product otoacoustic emissions at these ages (Sergeyenko et al., 2013)—the point of failure is likely to reside somewhere within IHCs and/or auditory nerve fibers. Remarkably, Kujawa and colleagues (2013) found that auditory nerve fibers began to uncouple from IHCs midway through the first year of life, and the progression of this synaptopathy was highly correlated with a change in response magnitude. A direct comparison with their results (specifically, see Fig. 5D of Sergeyenko et al., 2013) would suggest that approximately 20–25% of auditory nerve fibers have been silenced in our one-year-old mice, because Wave 1 amplitudes were just 50% of their 4-wk levels.

Curiously, nearly twice as many auditory nerve fibers are reported to disconnect from IHCs at the apical (lower frequency) end of the cochlea in mice by one year of age, although this loss begins to balance out in the second year (Sergeyenko et al., 2013). As the correspondence in the rate of decline between Wave 1 amplitude and percentage of IHC innervation has been suggested to be quite robust for multiple frequencies (Sergeyenko et al., 2013), we predicted greater reductions in Wave 1 amplitude at 52 wks for 8-kHz compared to 24-kHz in our dataset. Instead, after normalization, we saw nearly identical rates of decline over the course of a year for all tested stimuli, which would suggest the presumed underlying cochlear synaptopathy is occurring at similar rates throughout the cochlea. It is possible, however, that enhanced synaptopathy in the apex could have still occurred at 52 wks but that its presence, as predicted by Wave 1 amplitudes, was otherwise obscured by the recruitment of additional auditory nerve fibers along the cochlear spiral with low-frequency stimulation at suprathreshold levels (e.g., 80 dB SPL).

The second component of the ABR waveform has been associated, in cat, with the activation of globular BCs in the CN (Melcher and Kiang, 1996). While the presence of distinct BC subtypes in the mouse remains ambiguous (Lauer et al., 2013), it is reasonable to assume that Wave 2 in our data is generated by the activation of cells in the ventral CN including, but perhaps not limited to, BCs receiving EB inputs. In our results, Wave 2 amplitudes declined in concert with Wave 1, suggesting this secondary reduction is a direct reflection of reduced cochlear drive, rather than a separate manifestation of pathology at the central termination of auditory nerve fibers in the CN and/or their target cells. However, degraded signal transmission at the EB-BC synapse has been observed in very old (>2-yrs) CBA/CaJ mice (Xie, 2016; Xie and Manis, 2017), and it is possible that had we followed our subjects beyond a year, central dysfunction could have emerged secondary to cochlear synaptopathy and further compromised Wave 2 output.

Wave 5 (or V) is generally associated with activation of the auditory midbrain (Melcher and Kiang, 1996). The persistence or enhancement of Wave 5 magnitude relative to decreases in early waves (1 and 2) with age has been argued to reflect a homeostatic increase in neural "gain" in the central auditory nuclei in response to partial auditory nerve de-afferentation (Schaette and McAlpine, 2011). This transition is reflected in our results, where mean Wave 5:1 and 5:2 ratios increased ~2× and ~1.5×, respectively, over the course of a year. This increased drive in the absence of peripheral stimulation could be a potential source of phantom sound perception (i.e., tinnitus), which is a frequent complaint of aged individuals (Lockwood et al., 2002).

4.3. Endbulbs of Held

EBs and BCs play an essential role in preserving timing information used for sound localization (Grothe et al., 2010) and spectral processing (Shofner, 2008). Within their complex arborizations, EBs contain hundreds of active zones for coordinated neurotransmitter release (Nicol and Walmsley, 2002; Ryugo et al., 1996), making them capable of rapidly delivering auditory spikes to postsynaptic BCs with high fidelity and precision (Manis et al., 2011). A shrunken, less complex EB may result in less efficient activation of postsynaptic BCs (Walmsley et al., 1998). The importance of this unique auditory nerve ending for hearing is emphasized by its evolutionary constancy in vertebrates (Ryugo and Parks,

2003).

The coincident development of EB structure and function during the early postnatal period implies a close relationship between these two parameters: EB branching and complexity (Ryugo and Fekete, 1982; Ryugo et al., 2006) is correlated in time with increases in spike rate, synchronization of impulses, improvement in hearing threshold, and shortening of spike latency in the AVCN (Brugge et al., 1978, 1981; Kettner et al., 1985; Walsh and McGee, 1987, 1988; Walsh et al., 1986). While EB development prior to hearing-onset may be initially supported by spontaneous activity in the auditory nerve (Connelly et al., 2017; Tritsch et al., 2007, 2010), its maintenance clearly requires sound-evoked activity, as prolonged deafness consistently results in morphological atrophy (Connelly et al., 2017; Limb and Ryugo, 2000; Ryugo et al., 1997, 1998; Wright et al., 2014; Youssoufian et al., 2008), ultrastructural alterations (Gulley et al., 1978; Lee et al., 2003; Ryugo et al., 1997), and synaptic transmission irregularities (Oleskevich and Walmsley, 2002). This dependence on hearing is further reinforced by the rescue of normal morphology following electrical stimulation of the auditory nerve through cochlear implantation in deaf white cats (Ryugo et al., 2005).

Acquired sensorineural hearing loss can occur because of damage to sensory receptors in the cochlea (Schuknecht, 1974) and/or a loss of synaptic communication with their associated auditory nerve fibers (Liberman and Kujawa, 2017), but the net consequence is the same either way: a subset of neurons in the auditory nerve become functionally silent. Furthermore, these silenced neurons can persist for months following peripheral de-afferentation (Kujawa and Liberman, 2009; Sergeyenko et al., 2013; Stamataki et al., 2006). Data from studies of deafness suggest that EBs belonging to this silent fraction may also, in time, begin to exhibit pathological changes. The critical question is whether the EB is functionally connected to an IHC, or not? Short of reconstructing individual auditory nerve fibers end-to-end from the periphery to the CN—a near-impossible task even with current technology—this query cannot be answered directly. Instead, we make inferences based on particular patterns of hearing loss. For example, some studies have used the DBA/2 mouse, which begins to exhibit high-frequency hearing loss shortly after the onset of hearing (3–4 wks), and expands to broad-spectrum loss by adulthood (Willott and Erway, 1998; Zheng et al., 1999). This pattern of hearing loss is coupled to the progressive loss of hair cells (Hultcrantz and Spangberg, 1997) attributed to mutations in proteins critical to hair cell function (Noben-Trauth et al., 2003; Shin et al., 2010). By restricting analysis to a limited frequency region of the CN where the severity of hearing loss was graded with age, and therefore also the likelihood that a given EB was still activiated by sound, a progressive atrophy of EB morphology was observed that mirrored the severity of hearing loss (Connelly et al., 2017). Furthermore, a study of EB physiology in high- (hearing loss) and low- (normal hearing) frequency regions of these mice revealed irregularities in synaptic transmission as a consequence of diminished sound-evoked activity in the auditory nerve (Wang and Manis, 2005).

Unfortunately, the above approach is not so easily applied to the current study. Both anatomical and physiological evidence suggests that age-related synaptopathy in the first year of life occurs throughout the sensory epithelium of the CBA/Ca cochlea (Sergeyenko et al., 2013; current study). Accordingly, in our one-year-old cohort, it is possible that only ~25% of the EBs we studied belonged to silenced auditory nerve fibers, with the rest remaining functionally normal. This sampling could be further skewed by our blinded approach to analysis (see Section 2.5), and we may have biased our selection towards more obvious EBs, inadvertently bypassing severely atrophic EBs that are nearly indistinguishable from incompletely filled endings (Connelly et al., 2017). Ideally, we could have controlled for this potential bias by calculating EB density in the AVCN—assuming EBs do not disappear altogether, a reduced density in older animals might evidence a biased sampling strategy. Unfortunately, this approach was not feasible, as there was no guarantee that the uptake of tracer dye by AN fibers was complete and total, rendering such measurements ineffective. As a result, it is possible that the significant reductions we observed are underestimations of the true effect.

The decline in EB morphology resembles a moderate variant of the EB pathology observed in mice with more extreme forms of hearing loss (Connelly et al., 2017; Limb and Ryugo, 2000). Compared to normal hearing CBA/J mice, congenitally deaf *shaker-2*$^{-/-}$ mice exhibit a two-fold reduction in EB complexity at just 9 wks of age, as quantified by 2D fractal analysis (Limb and Ryugo, 2000). This strain also exhibits a ~40% reduction in 2D EB silhouette area at 12 wks (vs. 4 wks), followed by a significant drop in 2D EB shape factor—a different quantification of complexity—at 24 wks (Connelly et al., 2017). In contrast, early-onset progressive hearing loss in DBA/2 mice results in delayed morphological changes; a similar ~40% reduction in 2D EB silhouette area is not seen until 24 wks, and had these animals been followed beyond this age, it is likely that a significantly reduced 2D EB shape factor would soon follow (Connelly et al., 2017). In both aforementioned scenarios, the hearing loss is explicitly overt—EB pathology follows the elevation, or complete abolishment, of audiometric thresholds. We observed significant atrophy in EB morphology at 52 wks in CBA mice—even EBs from 40-wk old mice were comparable to earlier measurements—a situation that emphasizes the gradual effect of hidden hearing loss in otherwise normal hearing subjects. Taken together, observations from mice with varying levels of hearing loss support the idea that EB morphology is responsive to changes in auditory nerve activity.

A strict interpretation of the split between connected and disconnected peripheral auditory nerve endings might suggest a dichotomy in the distribution in our EB measurements. Although we observed a significant reduction in EB complexity at 52 wks (Fig. 7C), we found no statistical evidence for a bimodal distribution in any of our samples. A recent analysis of EB physiology in extremely old CBA/CaJ mice, where up to 50% of auditory nerve fibers may be disconnected from IHCs (Sergeyenko et al., 2013), commented on this lack of segregation in their data and suggested that the deterioration in synaptic transmission in aged mice may be a more generalized phenomenon (Xie and Manis, 2017). We did not examine ultrastructural features of EBs in this study, but it is expected that any changes in this regard might be minimal since scant ultrastructural pathology was observed in mice with more aggressive forms of acquired hearing loss (Connelly et al., 2017).

Myelinated auditory nerve fibers can be subdivided on the basis of their spontaneous firing rate (SR) and threshold of activation (Kiang et al., 1965; Liberman, 1978). A bimodal distribution of SRs is often observed, where 60–70% of fibers have high SRs (>30 spikes/s) and the remaining 30–40% have low SRs (<10 spikes/s; Evans and Palmer, 1980; Kiang et al., 1965; Liberman, 1978; Tsuji and Liberman, 1997). While a clear bimodal SR distribution is not apparent in mouse (Taberner and Liberman, 2005), the inverse relationship between SR and threshold is a constant: fibers with the highest SRs have the lowest thresholds. This distinction is reflected in the pattern of peripheral innervation, where low- and high-SR fibers contact the modiolar and pillar sides of IHCs, respectively (Liberman et al., 2015; Liberman, 1980, 1982). The central EB termination of auditory nerve fibers also displays characteristic differences based on SR: EBs emanating from low-SR fibers are consistently more complex than those of high-SR fibers (Ryugo et al., 1996; Sento and Ryugo, 1989; Tsuji and Liberman, 1997), and only EBs of the same SR-type converge onto a given BC (Sento

and Ryugo, 1989).

As noted above, we found no statistical support for bimodal distributions of endbulb complexity measurements at any age in our mice. However, given the lack of distinct populations of low- vs. high-SR responses in mouse (Taberner and Liberman, 2005), it is likely that our results reflect a corresponding gradient of high- to low-SR fibers. Interestingly, there is strong evidence that the cochlear synaptopathy of hidden hearing loss, due to either aging or noise-trauma, is largely selective for low-SR fibers (Furman et al., 2013; Liberman et al., 2015; Schmiedt et al., 1996; Stamataki et al., 2006). Accordingly, the downward shift in the mean and peak probability of EB complexity in our 52-wk animals (Fig. 7C) could reflect the selective atrophy of these normally more-complex low-SR EBs—the theoretical 25% fraction of silent fibers at one year (see above) may largely correspond to low-SR auditory nerve fibers, whereas the functional remainder contains both classes. Certainly, the most complex EBs in our dataset (shape factor >7) were only observed in younger cohorts. Whether selective for low-SR fibers or not, the reduction of EB complexity in our study further emphasizes the dependence of normal sound-evoked activity for maintenance of EB structure and function.

4.4. Functional implications

ABR thresholds are often regarded as a diagnostic for hearing health, and threshold elevations are certainly a harbinger of cochlear dysfunction and perceptual difficulties (Schuknecht, 1974). Yet, many symptoms of age-related hearing loss, such as complaints of poor audibility and speech intelligibility, can manifest without threshold shifts (Gordon-Salant, 2005). It has been speculated that we possess 10× more auditory nerve fibres than required to detect sounds (Ohlemiller and Frisina, 2008) and normal audiometric hearing thresholds can withstand a loss of up to 80% IHCs (Lobarinas et al., 2013) or auditory nerve fibers (Schuknecht and Woellner, 1953). Instead, a more sobering "hidden" variant of hearing loss has been revealed with the demonstration of cochlear synaptopathology in both noise-exposed (Furman et al., 2013; Kujawa and Liberman, 2009; Lin et al., 2011) and aged (Sergeyenko et al., 2013; Viana et al., 2015) subjects with normal audiometric thresholds. Our results reveal that this pathology is not limited to the cochlea, and could spread higher in the central auditory system, further compromising sound processing and perception.

The specific pattern of cochlear synaptopathy may partly explain some of the more confounding aspects of hearing loss. Low-SR fibers have higher thresholds and wider dynamic ranges than high-SR fibers (Winter et al., 1990), and are resistant to saturation at high noise levels (Costalupes et al., 1984). Low-SR fibers are also the exclusive source of primary input to the small cell cap of the CN, at least in cat (Ryugo, 2008). These cells have been implicated in a high-threshold feedback circuit for modulation of inner ear sensitivity (Ye et al., 2000). Accordingly, low-SR fibers may be critical for parsing sound signals in loud and noisy environments, and their selective vulnerability to noise and/or aging (Furman et al., 2013; Liberman et al., 2015; Schmiedt et al., 1996; Stamataki et al., 2006) may help explain why aged listeners have trouble understanding speech in background noise (Gordon-Salant, 2005).

Research on hidden hearing loss has re-focused attention on peripheral de-afferentation as a primary source of auditory pathology, even in cases where thresholds appear normal (Liberman and Kujawa, 2017). It remains unclear whether these peripheral losses can be reversed, either through spontaneous recovery (Puel et al., 1995; Song et al., 2016) or targeted therapy (Gunewardene et al., 2016). Any attempts at restoring function, however, must also consider that the consequences of this impairment could have propagated centrally over time. Our revelation of an age-related pathology in the endbulb of Held is likely secondary to hidden hearing loss in the periphery, but nonetheless is expected to compromise the processing of acoustic cues for sound localization and speech comprehension. Awareness of central abnormalities that accompany hearing loss following cochlear damage is mandatory if we are to develop effective therapeutic strategies for this condition.

Role of authors

The authors had full access to all the data in the study and take responsibility for the integrity of the data and accuracy of the analysis. Study concept and design: MAM, FEA, DKR. Acquisition of data: FEA. Analysis and interpretation of data: MAM, FEA, DKR. Drafting and revising the manuscript: MAM, FEA, DKR.

Declarations of interest

None.

Acknowledgements

The authors thank Catherine Connelly, Kiera Grierson, Giedre Milinkeviciute, and Kirupa Suthakar for sharing their ABR data, Timothy Peters for providing statistical advice, and the reviewers for their constructive comments on the manuscript. This work was supported by grants from the National Health and Medical Research Council (NHMRC; Grant nos.1080652 and 1081478), the Oticon Foundation (Grant no. 15-1814), the Walker Family Foundation, and gifts from Alan and Lynne Rydge, Haydn and Sue Daw, and the Rotary Club of Kings Cross.

Appendix A. Supplementary data

Supplementary data related to this article can be found at https://doi.org/10.1016/j.heares.2018.03.021.

References

Berlin, C.I., 1963. Hearing in mice via gsr audiometry. J. Speech Hear. Res. 6, 359–368.
Botev, Z.I., Grotowski, J.F., Kroese, D.P., 2010. Kernel density estimation via diffusion. Ann. Stat. 38, 2916–2957.
Breheny, P., Burchett, W., 2017. visreg: Visualization of Regression Models. https://CRAN.R-project.org/package=visreg.
Brugge, J.F., Javel, E., Kitzes, L.M., 1978. Signs of functional maturation of peripheral auditory system in discharge patterns of neurons in anteroventral cochlear nucleus of kitten. J. Neurophysiol. 41, 1557–1559.
Brugge, J.F., Kitzes, L.M., Javel, E., 1981. Postnatal development of frequency and intensity sensitivity of neurons in the anteroventral cochlear nucleus of kittens. Hear. Res. 5, 217–229.
Connelly, C.J., Ryugo, D.K., Muniak, M.A., 2017. The effect of progressive hearing loss on the morphology of endbulbs of Held and bushy cells. Hear. Res. 343, 14–33.
Costalupes, J.A., Young, E.D., Gibson, D.J., 1984. Effects of continuous noise backgrounds on rate response of auditory nerve fibers in cat. J. Neurophysiol. 51, 1326–1344.
DeHoff, R.T., 1978. Stereological uses of the area tangent count. In: Miles, R.E., Serra, J. (Eds.), Geometrical Probability and Biological Structures: Buffon's 200th Anniversary. Springer-Verlag, Berlin, pp. 99–113.
Dinno, A., 2017. dunn.test: Dunn's Test of Multiple Comparisons Using Rank Sums. https://CRAN.R-project.org/package=dunn.test.
Dubno, J.R., Dirks, D.D., Morgan, D.E., 1984. Effects of age and mild hearing loss on speech recognition in noise. J. Acoust. Soc. Am. 76, 87–96.
Evans, E.F., Palmer, A.R., 1980. Relationship between the dynamic-range of cochlear nerve-fibers and their spontaneous activity. Exp. Brain Res. 40, 115–118.
Fogarty, M.J., Hammond, L.A., Kanjhan, R., Bellingham, M.C., Noakes, P.G., 2013. A method for the three-dimensional reconstruction of Neurobiotin-filled neurons and the location of their synaptic inputs. Front. Neural Circ. 7, 153.
Frisina, D.R., Frisina, R.D., 1997. Speech recognition in noise and presbycusis: relations to possible neural mechanisms. Hear. Res. 106, 95–104.
Fullgrabe, C., Moore, B.C., Stone, M.A., 2014. Age-group differences in speech identification despite matched audiometrically normal hearing: contributions from auditory temporal processing and cognition. Front. Aging Neurosci. 6, 347.

Furman, A.C., Kujawa, S.G., Liberman, M.C., 2013. Noise-induced cochlear neuropathy is selective for fibers with low spontaneous rates. J. Neurophysiol. 110, 577–586.
Gordon-Salant, S., 2005. Hearing loss and aging: new research findings and clinical implications. J. Rehabil. Res. Dev. 42, 9–24.
Gordon-Salant, S., Fitzgibbons, P.J., 1993. Temporal factors and speech recognition performance in young and elderly listeners. J. Speech Hear. Res. 36, 1276–1285.
Grömping, U., 2006. Relative importance for linear regression in R: the package relaimpo. J. Stat. Software 17.
Grothe, B., Pecka, M., McAlpine, D., 2010. Mechanisms of sound localization in mammals. Physiol. Rev. 90, 983–1012.
Gulley, R.L., Wenthold, R.J., Neises, G.R., 1978. Changes in the synapses of spiral ganglion cells in the rostral anteroventral cochlear nucleus of the waltzing Guinea pig following hair cell loss. Brain Res. 158, 279–294.
Gunewardene, N., Crombie, D., Dottori, M., Nayagam, B.A., 2016. Innervation of cochlear hair cells by human induced pluripotent stem cell-derived neurons in vitro. Stem Cell. Int. 2016, 1781202.
Hashisaki, G.T., Rubel, E.W., 1989. Effects of unilateral cochlea removal on anteroventral cochlear nucleus neurons in developing gerbils. J. Comp. Neurol. 283, 5–73.
Held, H., 1893. Die centrale gehörleitung. Arch. Anat. Physiol. Anat. Abt. 201–248.
Henry, K.R., Lepkowski, C.M., 1978. Evoked potential correlates of genetic progressive hearing loss. Age-related changes from the ear to the inferior colliculus of C57BL/6 and CBA/J mice. Acta Otolaryngol. 86, 366–374.
Henry, K.R., Chole, R.A., 1980. Genotypic differences in behavioral, physiological and anatomical expressions of age-related hearing loss in the laboratory mouse. Audiologyogy 19, 369–383.
Hultcrantz, M., Spangberg, M.L., 1997. Pathology of the cochlea following a spontaneous mutation in DBA/2 mice. Acta Otolaryngol. 117, 689–695.
Johnson, K.R., Erway, L.C., Cook, S.A., Willott, J.F., Zheng, Q.Y., 1997. A major gene affecting age-related hearing loss in C57BL/6J mice. Hear. Res. 114, 83–92.
Kettner, R.E., Feng, J.Z., Brugge, J.F., 1985. Postnatal development of the phase-locked response to low frequency tones of auditory nerve fibers in the cat. J. Neurosci. 5, 275–283.
Kiang, N.Y.-S., Watanabe, T., Thomas, E.C., Clark, L.F., 1965. Discharge Patterns of Single Fibers in the Cat's Auditory Nerve. MIT Press, Cambridge, MA.
Kral, A., Tillein, J., Heid, S., Hartmann, R., Klinke, R., 2005. Postnatal cortical development in congenital auditory deprivation. Cerebr. Cortex 15, 552–562.
Kujawa, S.G., Liberman, M.C., 2009. Adding insult to injury: cochlear nerve degeneration after "temporary" noise-induced hearing loss. J. Neurosci. 29, 14077–14085.
Lauer, A.M., Connelly, C.J., Graham, H., Ryugo, D.K., 2013. Morphological characterization of bushy cells and their inputs in the laboratory mouse (Mus musculus) anteroventral cochlear nucleus. PLoS One 8, e73308.
Lee, D.J., Cahill, H.B., Ryugo, D.K., 2003. Effects of congenital deafness in the cochlear nuclei of Shaker-2 mice: an ultrastructural analysis of synapse morphology in the endbulbs of Held. J. Neurocytol. 32, 229–243.
Lenn, N.J., Reese, T.S., 1966. The fine structure of nerve endings in the nucleus of the trapezoid body and the ventral cochlear nucleus. Am. J. Anat. 118, 375–389.
Li, H.S., Borg, E., 1991. Age-related loss of auditory sensitivity in two mouse genotypes. Acta Otolaryngol. 111, 827–834.
Liberman, L.D., Suzuki, J., Liberman, M.C., 2015. Dynamics of cochlear synaptopathy after acoustic overexposure. J. Assoc. Res. Otolaryngol. 16, 205–219.
Liberman, M.C., 1978. Auditory-nerve response from cats raised in a low-noise chamber. J. Acoust. Soc. Am. 63, 442–455.
Liberman, M.C., 1980. Morphological differences among Radial afferent-fibers in the cat cochlea - an Electron-microscopic study of serial sections. Hear. Res. 3, 45–63.
Liberman, M.C., 1982. Single-neuron labeling in the cat auditory nerve. Science 216, 1239–1241.
Liberman, M.C., Kujawa, S.G., 2017. Cochlear synaptopathy in acquired sensorineural hearing loss: manifestations and mechanisms. Hear. Res. 349, 138–147.
Limb, C.J., Ryugo, D.K., 2000. Development of primary axosomatic endings in the anteroventral cochlear nucleus of mice. J. Assoc. Res. Otolaryngol. 1, 103–119.
Lin, H.W., Furman, A.C., Kujawa, S.G., Liberman, M.C., 2011. Primary neural degeneration in the Guinea pig cochlea after reversible noise-induced threshold shift. J. Assoc. Res. Otolaryngol. 12, 605–616.
Lindeman, R.H., Merenda, P.F., Gold, R.Z., 1980. Introduction to Bivariate and Multivariate Analysis. Scott Foresman & Co, Glenview, IL.
Lobarinas, E., Salvi, R., Ding, D., 2013. Insensitivity of the audiogram to carboplatin induced inner hair cell loss in chinchillas. Hear. Res. 302, 113–120.
Lockwood, A.H., Salvi, R.J., Burkard, R.F., 2002. Tinnitus. N. Engl. J. Med. 347, 904–910.
Lorente de Nó, R., 1981. The Primary Acoustic Nuclei. Raven Press, New York.
Lorenzi, C., Gilbert, G., Carn, H., Garnier, S., Moore, B.C., 2006. Speech perception problems of the hearing impaired reflect inability to use temporal fine structure. Proc. Natl. Acad. Sci. U. S. A. 103, 18866–18869.
Maechler, M., 2016. Diptest: Hartigan's Dip Test Statistic for Unimodality - Corrected. https://CRAN.R-project.org/package=diptest.
Manis, P.B., Xie, R., Wang, Y., Marrs, G.S., Spirou, G.A., 2011. The endbulbs of held. In: Trussell, L.O., Popper, A.N., Fay, R.R. (Eds.), Synaptic Mechanisms in the Auditory System. Springer, New York, pp. 61–93.
Melcher, J.R., Kiang, N.Y., 1996. Generators of the brainstem auditory evoked potential in cat. III: identified cell populations. Hear. Res. 93, 52–71.
Moore, D.R., Kowalchuk, N.E., 1988. Auditory brainstem of the ferret: effects of unilateral cochlear lesions on cochlear nucleus volume and projections to the inferior colliculus. J. Comp. Neurol. 272, 503–515.
Muniak, M.A., Connelly, C.J., Suthakar, K., Milinkeviciute, G., Ayeni, F.E., Ryugo, D.K., 2016. Central projections of spiral ganglion neurons. In: Dabdoub, A., Fritzsch, B., Popper, A.N., Fay, R.R. (Eds.), The Primary Auditory Neurons of the Mammalian Cochlea. Springer, New York, pp. 157–190.
Ngodup, T., Goetz, J.A., McGuire, B.C., Sun, W., Lauer, A.M., Xu-Friedman, M.A., 2015. Activity-dependent, homeostatic regulation of neurotransmitter release from auditory nerve fibers. Proc. Natl. Acad. Sci. U. S. A. 112, 6479–6484.
Nicol, M.J., Walmsley, B., 2002. Ultrastructural basis of synaptic transmission between endbulbs of Held and bushy cells in the rat cochlear nucleus. J. Physiol. 539, 713–723.
Noben-Trauth, K., Zheng, Q.Y., Johnson, K.R., 2003. Association of cadherin 23 with polygenic inheritance and genetic modification of sensorineural hearing loss. Nat. Genet. 35, 21–23.
Ohlemiller, K.K., Frisina, R.D., 2008. Clinical characterization of age-related hearing loss and its neural and molecular bases. In: Schact, J., Popper, A.N., Fay, R.R. (Eds.), Auditory Trauma, Protection, and Repair. Springer, New York, pp. 145–194.
Ohlemiller, K.K., Jones, S.M., Johnson, K.R., 2016. Application of mouse models to research in hearing and balance. J. Assoc. Res. Otolaryngol. 17, 493–523.
Oleskevich, S., Walmsley, B., 2002. Synaptic transmission in the auditory brainstem of normal and congenitally deaf mice. J. Physiol. 540, 447–455.
Parham, K., 1997. Distortion product otoacoustic emissions in the C57BL/6J mouse model of age-related hearing loss. Hear. Res. 112, 216–234.
Parks, T.N., Rubel, E.W., Fay, R.R., Popper, A.N. (Eds.), 2004. Plasticity of the Auditory System. Springer, New York.
Powell, T.P., Erulkar, S.D., 1962. Transneuronal cell degeneration in the auditory relay nuclei of the cat. J. Anat. 96, 249–268.
Puel, J.L., Saffiedine, S., Gervais d'Aldin, C., Eybalin, M., Pujol, R., 1995. Synaptic regeneration and functional recovery after excitotoxic injury in the Guinea pig cochlea. C R Acad Sci III 318, 67–75.
R Core Team, 2017. R: a Language and Environment for Statistical Computing. https://www.R-project.org/.
Ronneberger, O., Baddeley, D., Scheipl, F., Verveer, P.J., Burkhardt, H., Cremer, C., Fahrmeir, L., Cremer, T., Joffe, B., 2008. Spatial quantitative analysis of fluorescently labeled nuclear structures: problems, methods, pitfalls. Chromosome Res. 16, 523–562.
Ruggles, D., Bharadwaj, H., Shinn-Cunningham, B.G., 2012. Why middle-aged listeners have trouble hearing in everyday settings. Curr. Biol. 22, 1417–1422.
Ryugo, D.K., 2008. Projections of low spontaneous rate, high threshold auditory nerve fibers to the small cell cap of the cochlear nucleus in cats. Neuroscience 154, 114–126.
Ryugo, D.K., Fekete, D.M., 1982. Morphology of primary axosomatic endings in the anteroventral cochlear nucleus of the cat: a study of the endbulbs of Held. J. Comp. Neurol. 210, 239–257.
Ryugo, D.K., Parks, T.N., 2003. Primary innervation of the avian and mammalian cochlear nucleus. Brain Res. Bull. 60, 435–456.
Ryugo, D.K., Spirou, G.A., 2009. Auditory system: giant synaptic terminals, endbulbs, and calyces. In: Squire, L.R. (Ed.), Encyclopedia of Neuroscience, vol. 1. Academic Press, Oxford, pp. 759–770.
Ryugo, D.K., Wu, M.M., Pongstaporn, T., 1996. Activity-related features of synapse morphology: a study of endbulbs of held. J. Comp. Neurol. 365, 141–158.
Ryugo, D.K., Kretzmer, E.A., Niparko, J.K., 2005. Restoration of auditory nerve synapses in cats by cochlear implants. Science 310, 1490–1492.
Ryugo, D.K., Pongstaporn, T., Huchton, D.M., Niparko, J.K., 1997. Ultrastructural analysis of primary endings in deaf white cats: morphologic alterations in endbulbs of Held. J. Comp. Neurol. 385, 230–244.
Ryugo, D.K., Rosenbaum, B.T., Kim, P.J., Niparko, J.K., Saada, A.A., 1998. Single unit recordings in the auditory nerve of congenitally deaf white cats: morphological correlates in the cochlea and cochlear nucleus. J. Comp. Neurol. 397, 532–548.
Ryugo, D.K., Montey, K.L., Wright, A.L., Bennett, M.L., Pongstaporn, T., 2006. Postnatal development of a large auditory nerve terminal: the endbulb of Held in cats. Hear. Res. 216–217, 100–115.
Saada, A.A., Niparko, J.K., Ryugo, D.K., 1996. Morphological changes in the cochlear nucleus of congenitally deaf white cats. Brain Res. 736, 315–328.
Schaette, R., McAlpine, D., 2011. Tinnitus with a normal audiogram: physiological evidence for hidden hearing loss and computational model. J. Neurosci. 31, 13452–13457.
Schmiedt, R.A., Mills, J.H., Boettcher, F.A., 1996. Age-related loss of activity of auditory-nerve fibers. J. Neurophysiol. 76, 2799–2803.
Schuknecht, H.F., 1974. Pathology of the Ear. Harvard University Press, Cambridge.
Schuknecht, H.F., Woellner, R.C., 1953. Hearing losses following partial section of the cochlear nerve. Laryngoscope 63, 441–465.
Schwartz, I.R., Higa, J.F., 1982. Correlated studies of the ear and brainstem in the deaf white cat: changes in the spiral ganglion and the medial superior olivary nucleus. Acta Otolaryngol. 93, 9–18.
Sento, S., Ryugo, D.K., 1989. Endbulbs of held and spherical bushy cells in cats: morphological correlates with physiological properties. J. Comp. Neurol. 280, 553–562.
Sergeyenko, Y., Lall, K., Liberman, M.C., Kujawa, S.G., 2013. Age-related cochlear synaptopathy: an early-onset contributor to auditory functional decline. J. Neurosci. 33, 13686–13694.
Shin, J.B., Longo-Guess, C.M., Gagnon, L.H., Saylor, K.W., Dumont, R.A., Spinelli, K.J., Pagana, J.M., Wilmarth, P.A., David, L.L., Gillespie, P.G., Johnson, K.R., 2010. The

R109H variant of fascin-2, a developmentally regulated actin crosslinker in hair-cell stereocilia, underlies early-onset hearing loss of DBA/2J mice. J. Neurosci. 30, 9683–9694.
Shofner, W.P., 2008. Representation of the spectral dominance region of pitch in the steady-state temporal discharge patterns of cochlear nucleus units. J. Acoust. Soc. Am. 124, 3038–3052.
Snell, K.B., Frisina, D.R., 2000. Relationships among age-related differences in gap detection and word recognition. J. Acoust. Soc. Am. 107, 1615–1626.
Song, Q., Shen, P., Li, X., Shi, L., Liu, L., Wang, J., Yu, Z., Stephen, K., Aiken, S., Yin, S., Wang, J., 2016. Coding deficits in hidden hearing loss induced by noise: the nature and impacts. Sci. Rep. 6, 25200.
Spongr, V.P., Flood, D.G., Frisina, R.D., Salvi, R.J., 1997. Quantitative measures of hair cell loss in CBA and C57BL/6 mice throughout their life spans. J. Acoust. Soc. Am. 101, 3546–3553.
Stamataki, S., Francis, H.W., Lehar, M., May, B.J., Ryugo, D.K., 2006. Synaptic alterations at inner hair cells precede spiral ganglion cell loss in aging C57BL/6J mice. Hear. Res. 221, 104–118.
Taberner, A.M., Liberman, M.C., 2005. Response properties of single auditory nerve fibers in the mouse. J. Neurophysiol. 93, 557–569.
Tritsch, N.X., Yi, E., Gale, J.E., Glowatzki, E., Bergles, D.E., 2007. The origin of spontaneous activity in the developing auditory system. Nature 450, 50–55.
Tritsch, N.X., Rodriguez-Contreras, A., Crins, T.T., Wang, H.C., Borst, J.G., Bergles, D.E., 2010. Calcium action potentials in hair cells pattern auditory neuron activity before hearing onset. Nat. Neurosci. 13, 1050–1052.
Trune, D.R., 1982. Influence of neonatal cochlear removal on the development of mouse cochlear nucleus: I. Number, size, and density of its neurons. J. Comp. Neurol. 209, 409–424.
Tsuji, J., Liberman, M.C., 1997. Intracellular labeling of auditory nerve fibers in Guinea pig: central and peripheral projections. J. Comp. Neurol. 381, 188–202.
Viana, L.M., O'Malley, J.T., Burgess, B.J., Jones, D.D., Oliveira, C.A., Santos, F., Merchant, S.N., Liberman, L.D., Liberman, M.C., 2015. Cochlear neuropathy in human presbycusis: confocal analysis of hidden hearing loss in post-mortem tissue. Hear. Res. 327, 78–88.
Walmsley, B., Alvarez, F.J., Fyffe, R.E., 1998. Diversity of structure and function at mammalian central synapses. Trends Neurosci. 21, 81–88.
Walsh, E.J., McGee, J., 1987. Postnatal development of auditory nerve and cochlear nucleus neuronal responses in kittens. Hear. Res. 28, 97–116.
Walsh, E.J., McGee, J., 1988. Rhythmic discharge properties of caudal cochlear nucleus neurons during postnatal development in cats. Hear. Res. 36, 233–247.
Walsh, E.J., McGee, J., Javel, E., 1986. Development of auditory-evoked potentials in the cat. I. Onset of response and development of sensitivity. J. Acoust. Soc. Am. 79, 712–724.
Wang, Y., Manis, P.B., 2005. Synaptic transmission at the cochlear nucleus endbulb synapse during age-related hearing loss in mice. J. Neurophysiol. 94, 1814–1824.
Wang, Y., Manis, P.B., 2006. Temporal coding by cochlear nucleus bushy cells in DBA/2J mice with early onset hearing loss. J. Assoc. Res. Otolaryngol. 7, 412–424.
West, C.D., Harrison, J.M., 1973. Transneuronal cell atrophy in the congenitally deaf white cat. J. Comp. Neurol. 151, 377–398.
Willott, J.F., 1984. Changes in frequency representation in the auditory system of mice with age-related hearing impairment. Brain Res. 309, 159–162.
Willott, J.F., 1986. Effects of aging, hearing loss, and anatomical location on thresholds of inferior colliculus neurons in C57BL/6 and CBA mice. J. Neurophysiol. 56, 391–408.
Willott, J.F., Erway, L.C., 1998. Genetics of age-related hearing loss in mice. IV. Cochlear pathology and hearing loss in 25 BXD recombinant inbred mouse strains. Hear. Res. 119, 27–36.
Willott, J.F., Parham, K., Hunter, K.P., 1991. Comparison of the auditory sensitivity of neurons in the cochlear nucleus and inferior colliculus of young and aging C57BL/6J and CBA/J mice. Hear. Res. 53, 78–94.
Winter, I.M., Robertson, D., Yates, G.K., 1990. Diversity of characteristic frequency rate-intensity functions in Guinea pig auditory nerve fibres. Hear. Res. 45, 191–202.
Wright, S., Hwang, Y., Oertel, D., 2014. Synaptic transmission between end bulbs of Held and bushy cells in the cochlear nucleus of mice with a mutation in Otoferlin. J. Neurophysiol. 112, 3173–3188.
Xie, R., 2016. Transmission of auditory sensory information decreases in rate and temporal precision at the endbulb of Held synapse during age-related hearing loss. J. Neurophysiol. 116, 2695–2705.
Xie, R., Manis, P.B., 2017. Synaptic transmission at the endbulb of Held deteriorates during age-related hearing loss. J. Physiol. 595, 919–934.
Ye, Y., Machado, D.G., Kim, D.O., 2000. Projection of the marginal shell of the anteroventral cochlear nucleus to olivocochlear neurons in the cat. J. Comp. Neurol. 420, 127–138.
Youssoufian, M., Couchman, K., Shivdasani, M.N., Paolini, A.G., Walmsley, B., 2008. Maturation of auditory brainstem projections and calyces in the congenitally deaf (dn/dn) mouse. J. Comp. Neurol. 506, 442–451.
Zeilhofer, H.U., Studler, B., Arabadzisz, D., Schweizer, C., Ahmadi, S., Layh, B., Bosl, M.R., Fritschy, J.M., 2005. Glycinergic neurons expressing enhanced green fluorescent protein in bacterial artificial chromosome transgenic mice. J. Comp. Neurol. 482, 123–141.
Zheng, Q.Y., Johnson, K.R., Erway, L.C., 1999. Assessment of hearing in 80 inbred strains of mice by ABR threshold analyses. Hear. Res. 130, 94–107.
Zhuang, X., Sun, W., Xu-Friedman, M.A., 2017. Changes in properties of auditory nerve synapses following conductive hearing loss. J. Neurosci. 37, 323–332.